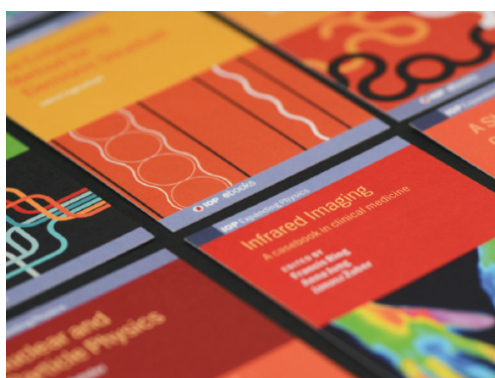


PAPER • OPEN ACCESS

Characterising stochastic motion in heterogeneous media driven by coloured non-Gaussian noise

To cite this article: Nicholas Mwilu Mutothya *et al* 2021 *J. Phys. A: Math. Theor.* **54** 295002

View the [article online](#) for updates and enhancements.



IOP | ebooks™

Bringing together innovative digital publishing with leading authors from the global scientific community.

Start exploring the collection—download the first chapter of every title for free.

Characterising stochastic motion in heterogeneous media driven by coloured non-Gaussian noise

Nicholas Mwilu Mutothya^{1,2}, Yong Xu^{1,*} , Yongge Li^{1,*} and Ralf Metzler^{3,*} 

¹ School of Mathematics and Statistics, Northwestern Polytechnical University, Xi'an, 710072, People's Republic of China

² Department of Mathematics and Informatics, Taita Taveta University, PO Box 635-80300 Voi, Kenya

³ University of Potsdam, Institute of Physics & Astronomy, 14476 Potsdam, Germany

E-mail: rmetzler@uni-potsdam.de, liyonge@nwpu.edu.cn and hsux3@nwpu.edu.cn

Received 6 January 2021, revised 5 April 2021

Accepted for publication 26 April 2021

Published 29 June 2021



CrossMark

Abstract

We study the stochastic motion of a test particle in a heterogeneous medium in terms of a position dependent diffusion coefficient mimicking measured deterministic diffusivity gradients in biological cells or the inherent heterogeneity of geophysical systems. Compared to previous studies we here investigate the effect of the interplay of anomalous diffusion effected by position dependent diffusion coefficients and coloured non-Gaussian noise. The latter is chosen to be distributed according to Tsallis' q -distribution, representing a popular example for a non-extensive statistic. We obtain the ensemble and time averaged mean squared displacements for this generalised process and establish its non-ergodic properties as well as analyse the non-Gaussian nature of the associated displacement distribution. We consider both non-stratified and stratified environments.

Keywords: diffusion, anomalous diffusion, non-extensive statistics, coloured noise, heterogeneous diffusion process

(Some figures may appear in colour only in the online journal)

*Authors to whom any correspondence should be addressed.



Original content from this work may be used under the terms of the [Creative Commons Attribution 4.0 licence](https://creativecommons.org/licenses/by/4.0/). Any further distribution of this work must maintain attribution to the author(s) and the title of the work, journal citation and DOI.

1. Introduction

Since its classical probabilistic formulations by Einstein [1] and Smoluchowski [2], Brownian motion [3] emerged as a cornerstone of non-equilibrium statistical physics and physical kinetics [4, 5]. A central idea was the concept of fluctuating forces [6] originally phrased by Langevin in his description of Brownian motion based on the extension of Newton's second law [7]. The defining properties of Brownian motion in the continuum limit are the Gaussian probability density function (PDF) for finding the test particle at a given distance away from its initial position after a given time, and the linear growth in time of the mean squared displacement (MSD) [8, 9]. Applications of Brownian motion range from the modelling of molecular regulation dynamics in biological cells [10–12], modelling of stock and option markets price fluctuations [13], describing microbial evolution in predictive microbiology [14] to quantitative descriptions of tracer spreading on geophysical scales [15].

Deviations from the laws of Brownian motion in stochastic transport date back to Richardson's study of tracer dispersion in turbulent flows [16]. Another milestone was the study by Scher and Montroll, of diffusive charge carrier motion in amorphous semiconductors [17]. By now such 'anomalous diffusion', characterised by the non-linear time dependence $\langle x^2(t) \rangle \simeq K_\alpha t^\alpha$ of the MSD [18–22], is widely observed. Depending on the value of the anomalous diffusion exponent α one distinguishes subdiffusion ($0 < \alpha < 1$) and superdiffusion ($\alpha > 1$), and K_α of dimension $\text{cm}^2/\text{sec}^\alpha$ is the generalised diffusion coefficient [23]. Anomalous diffusion has been particularly well studied in biologically relevant systems [20, 24–26]. Subdiffusion, *inter alia*, was found for the motion of messenger RNA and lipid granules in live cells [27–29], telomeres in nuclei of mammalian cells [30], or the motion of lipids and proteins in membranes [31, 32]. Subdiffusion is also ubiquitous in subsurface hydrology [33, 34]. Superdiffusion, due to active molecular motion, is known from several cellular systems, *e.g.*, [35–38]. We also note that 'hyperdiffusion' with $\alpha > 2$ may occur, *e.g.*, in scenarios of tilted washboard potentials or in turbulence [16, 39].

Various theoretical models have been designed to describe different physical mechanisms underlying anomalous diffusion. Subdiffusive motion emerges, *e.g.*, from the continuous time random walk model with scale-free, power-law density of waiting times [17–20, 23, 41], as seen, *e.g.*, in membrane protein motion [42]. Another mechanism are long ranged correlations of the displacements, as in fractional Brownian motion (FBM) [43–48] or in fractional Langevin equation motion [49]. Such correlations are associated with the viscoelasticity of the environment and are observed, *e.g.*, in tracer diffusion in complex liquids [50] and in the crowded cytoplasm of biological cells and membranes [28, 32, 35, 42, 51–53]. Superdiffusion motion, *e.g.*, comes about due to positive correlations in FBM [43] or in spatiotemporally coupled Lévy walks [41, 54–61]. Examples for such statistics are found, *i.a.*, in correlated vesicle motion in cells [37] or for the motion of molecular motors in cells [38, 62]. A number of other anomalous diffusion models are described in [21, 23, 63].

Typically (anomalous) diffusion models are formulated with a fixed diffusion coefficient. In some specific systems, two or multiple different, quenched layers with different diffusivities are considered, *e.g.*, in the modelling of protein diffusion in bacterial cytoplasm and nucleoid region [11, 12]. Similarly, different approaches exist to quantify the motion of tracers in patchy landscapes with different diffusivities [64–67] as well as in quenched, rugged energy landscapes [21, 68]. Another, 'annealed' approach to heterogeneous environments is the concept of 'diffusing diffusivity' [69–76], in which the stochastic motion of the test particle is modulated by a time dependent diffusion coefficient, whose dynamics itself is a stochastic process, compare also the recent study demonstrating the fluctuating diffusivity of a protein

effected by its shape fluctuations [77]. The diffusing diffusivity concept was developed to describe experiments with linear ('Fickian') MSD but non-Gaussian displacement PDF that, ultimately, crosses over to an effective Gaussian. Such 'Brownian yet non-Gaussian' diffusion was observed in various systems [62, 78], see also the references in [72–76]. We note that the emergence of Brownian yet non-Gaussian diffusion was recently scrutinised on quenched diffusivity landscapes [79] and related to random coefficient autoregressive processes [80]. For anomalous diffusion with anticorrelated increments observed experimentally non-Gaussian statistics were also found [52, 53, 81, 82]. A formulation of FBM with diffusing diffusivity showed model-specific crossover behaviours [83, 84], while non-Gaussianity for generalised Langevin equations was studied in [85]. We also note generalisations in which the diffusivity is a functional of Brownian motion [86, 87].

Another class of systems considers 'deterministic heterogeneity' in the sense that the diffusion coefficient varies systematically as some prescribed function $D(x)$ [88–91]. A prime example for this behaviour is the diffusivity landscape mapped out in mammalian HeLa and NLFK cells, in which the local diffusivity of the tracers follows a quite clear increase from the cell boundary towards the cell nucleus [92], see also the study for bacteria cells in [93]. This is the case we study here. Concrete functional forms for $D(x)$ are power-law dependencies as well as logarithmic and exponential variations [88, 94–97]. The dynamics of these heterogeneous diffusion processes (HDPs) is anomalous and non-ergodic in the sense that ensemble and time averages of the MSD do not converge even asymptotically [88, 94, 98]. Moreover, HDP dynamics is ageing and leads to an emerging population splitting between high and low mobility tracer fractions [88, 95].

Some recent experimental and theoretical studies have given strong indications of non-Gaussian noise in the sensory systems in a type of crayfish [98], in rat skin [99], and in neural networks [100, 101]. The source of noise in many biological systems may be non-Gaussian [102–104]. Non-Gaussian diffusion in heterogeneous media has been discussed, specifically in the context of diffusing diffusivity models [79, 102]. We here generalise HDPs with power-law diffusivity dependence on the position of the test particle with regard to both autocorrelation and distribution of the input noise. Specifically we introduce an exponential noise–noise correlation, so-called coloured noise, and we consider non-Gaussian noise following Tsallis' q -distribution. As we will see these changes effect interesting new dynamics to HDPs and may be useful for a range of applications.

Coloured noise as we will apply here with exponential noise–noise correlation and thus finite correlation time have a quite long tradition in the theory of stochastic processes [105–108] and were originally considered in connection with lasers and magnetic resonance phenomena [108–111]. More recent applications of coloured noise include population dynamics [112] or neuron models [101–113]. Exponentially correlated noise is usually generated by an Ornstein–Uhlenbeck process [114–122]. Such a noise process depends on two parameters, the correlation time and the noise intensity. In the limit of zero correlation time the autocorrelation function approaches the delta function of white noise [123]. The distribution of coloured noise is typically assumed to be Gaussian.

Non-Gaussian noise will be modelled in terms of the Tsallis q -Gaussian or q -distribution [124, 125]. This distribution follows from Tsallis' non-extensive entropy [126, 127] and arises as solution of non-linear Fokker–Planck equations (FPE) [128]. Such types of distributions were observed in a wide variety of systems, such as financial markets [129, 130], granular media [131], or earthquake statistics [132]. The q -Gaussian emerges as a limit of highly correlated random variables [133]. Such non-extensive characteristics sometimes concurrently also exhibit long correlations or memory [134]. This type of noise is called coloured non-Gaussian

noise and can be generated from Tsallis’ q -Gaussian statistic. It can be viewed as a generalisation of the Ornstein–Uhlenbeck noise with a non-extensivity parameter q indicating the degree of departure from Gaussian [135, 136].

When the noise is Gaussian, HDPs are Markovian and analytical results can be obtained from the associated FPE [88]. For coloured non-Gaussian noise the process is non-Markovian and thus difficult to solve for analytical results [134]. However the problem can be transformed into a two-dimensional Markovian process which describes the joint dynamics of the stochastic and the noise processes. An effective Markov FPE can be obtained from approximate methods, including path integral methods [135, 137, 138] and the unified coloured noise approximation [137, 139]. The second order moment method can be applied to analyse non-Gaussian noise driven stochastic systems [140]. Studies using coloured non-Gaussian noise found that the departure of the noise from a Gaussian statistic significantly affects the response of the system, e.g., it enhances the signal to noise ratio in stochastic resonance, the current and efficiency in Brownian motors, or the trapping in resonant gating, and it shifts noise-induced transition lines [136, 141, 142].

We here study the dynamical properties of diffusion process driven by coloured non-Gaussian noise and with a position dependent diffusion coefficient. In particular, the behaviour of the time averaged and ensemble MSD is examined. Ergodicity breaking (EB) and non-Gaussianity effects are investigated. The paper is organised as follows. In section 2 we lay out the governing equations of the system and the employed numerical discretisation scheme as well as introduce definitions of the observable quantities. In section 3 we present and discuss our results. Specifically, the PDF is derived via the moment approach, the numerical simulations strategy is presented, and then the ensemble and time average MSD, as well as the EB and non-Gaussianity parameters are analysed. In section 4 we present our conclusions.

2. Model description

We here describe our model of diffusion in a heterogeneous medium, in which the diffusivity varies spatially and the driving noise is coloured and non-Gaussian.

2.1. Dynamical equations

Consider the following one-dimensional system for the displacement $x(t)$ of a test particle that is driven by the coloured non-Gaussian noise $\eta(t)$ (the ‘ q -noise’ [141]),

$$\frac{dx(t)}{dt} = \sqrt{2D(x)} \times \eta(t), \tag{1}$$

$$\frac{d\eta(t)}{dt} = -\frac{1}{\tau} \frac{d}{d\eta} V_q(\eta) + \frac{1}{\tau} \xi(t). \tag{2}$$

Here $\xi(t)$ represents Gaussian white noise of zero mean and correlation function $\langle \xi(t)\xi(t') \rangle = 2D\delta(t - t')$. τ is the characteristic time of the coloured non-Gaussian noise and the q -noise potential $V_q(\eta)$ is given by

$$V_q(\eta) = \frac{1}{\beta(q-1)} \log \left[1 + \beta(q-1) \frac{\eta^2}{2} \right], \tag{3}$$

with $\beta = \frac{\tau}{D}$. The index q is called the non-extensivity parameter, indicating the departure from Gaussian behaviour ($q = 1$ and $q \neq 1$ for Gaussian and non-Gaussian statistic, respectively). The diffusivity $D(x)$ in (1) is spatially dependent and varies as power-law of the form

$D(x) = D_0|x|^\alpha$ with exponent α . Several recent studies have considered such diffusivities with either constant or variable [95, 114] power-law exponent. To avert trapping of the particle due to the singularity at the origin $x = 0$ (zero or diverging diffusivity, depending on the scaling exponent α) in the numerical simulations we consider the diffusivity of the form

$$D(x) = \begin{cases} D_0(a + |x|^\alpha), & \text{for } \alpha > 0, \\ D_0/(a + |x|^\alpha), & \text{for } \alpha < 0, \end{cases} \tag{4}$$

with sufficiently small shift a [88, 95]. The exponent α assumes real values. The diffusivity is a constant for $\alpha = 0$, which implies a homogeneous diffusion process. For $\alpha > 0$, the diffusivity increases with increasing $|x|$, and conversely for $\alpha < 0$. We interpret the stochastic integral corresponding to the Langevin equation (1) in the Stratonovich sense [88]. This interpretation is permitted as long as we do not require the system to reach equilibrium, e.g., on a finite domain or in a confining external potential [91, 143, 144]. In particular, we note that the motion of tracers in biological cells, spreading patterns of animals or humans, or dynamics in financial mathematics, are typically far from equilibrium.

Note that the q -noise (2) is a generalisation of the Ornstein–Uhlenbeck process which renders the system non-Markovian. The statistical properties of the noise process $\eta(t)$ were discussed in [135, 141]. By solving the corresponding FPE, the stationary distribution $P_q^{\text{st}}(\eta)$ can be obtained. $P_q^{\text{st}}(\eta)$ is well defined only for $q \in (-\infty, 3)$ while for $q \geq 3$ it is not normalisable and thus not a valid PDF. For $q \in (1, 3)$ it reads

$$P_q^{\text{st}}(\eta) = \frac{1}{Z_q} \left[1 + \beta(q - 1) \frac{\eta^2}{2} \right]^{-1/(q-1)}, \quad \eta \in (-\infty, \infty), \tag{5}$$

with normalisation factor $Z_q = [\pi/(\beta[q - 1])]^{1/2} \Gamma(1/[q - 1] - 1/2) / \Gamma(1/[q - 1])$ where Γ indicates the Gamma function. For $q = 1$ it reads

$$P_1^{\text{st}}(\eta) = \frac{1}{Z_1} \exp(-\beta\eta^2/2), \tag{6}$$

with normalisation factor $Z_1 = \sqrt{\pi/\beta}$. This corresponds to Ornstein–Uhlenbeck noise. Finally for $q \in (-\infty, 1)$, the stationary PDF is given by

$$P_q^{\text{st}}(\eta) = \begin{cases} \frac{1}{Z_q} \left[1 - \left(\frac{\eta}{w} \right)^2 \right]^{1/(1-q)}, & \text{if } |\eta| < w, \\ 0, & \text{otherwise,} \end{cases} \tag{7}$$

with normalisation factor $Z_q = \sqrt{\pi/(\beta(1 - q))} \Gamma(1/[1 - q] + 1) / \Gamma(1/[1 - q] + 3/2)$. Here $w = [(1 - q)\beta/2]^{-1/2}$ is a cutoff value. The stationary distribution exists only for $q < 3$ (since for $q \geq 3$, Z_q diverges or is negative and consequently $P_q^{\text{st}}(\eta) < 0$ which means that it is not a PDF). The Ornstein–Uhlenbeck process, i.e., the process giving rise to Gaussian coloured noise, is recovered in the limit $q \rightarrow 1$. For $1 < q < \frac{5}{3}$ the distribution is fat-tailed while $q < 1$ yield cut-off distributions. The first moment vanishes, $\langle \eta(t) \rangle = 0$, while the second moment is finite only when $q < \frac{5}{3}$, for which it reads $\langle \eta(t)^2 \rangle = \frac{2D}{\tau(5-3q)}$.

2.2. Numerical discretisation scheme

For the simulations we employ a discrete representation based on Heun’s method, which is a second order Runge–Kutta-type integration scheme. We first rewrite the stochastic

equations (1) and (2) in the form

$$\frac{dx(t)}{dt} = f(x(t), \eta(t)), \tag{8}$$

$$\frac{d\eta(t)}{dt} = h(\eta(t), q) + \frac{1}{\tau}\xi(t), \tag{9}$$

where $f(x(t), \eta(t)) = \sqrt{2D(x(t))} \times \eta(t)$ and $h(\eta, q) = -\frac{1}{\tau} \left[\frac{2\eta(t)}{2+\eta(t)^2(q-1)\beta} \right]$. Then, the numerical iteration scheme reads

$$x(i+1) = x(i) + \Delta t \times \frac{[F_1(i) + F_2(i)]}{2}, \tag{10}$$

$$\eta(i+1) = \eta(i) + \Delta t \times \frac{[H_1(i) + H_2(i)]}{2} + \sqrt{\frac{2D \times \Delta t}{\tau^2}} \times R, \tag{11}$$

where R is a normally distributed random variable with zero mean and unit variance, and

$$F_1(i) = \sqrt{2D[x(i)]} \times \eta(i), \tag{12}$$

$$F_2(i) = \sqrt{2 \{D[x(i)] + \Delta t \times F_1(i)\}} \times \left(\eta(i) + H_1(i)\Delta t + \sqrt{\frac{2D \times \Delta t}{\tau^2}} \times R \right), \tag{13}$$

$$H_1(i) = -\frac{2\eta(i)/\tau}{2 + \eta(i)^2 \times (q-1) \times \beta}, \tag{14}$$

$$H_2(i) = -\frac{2 \left[\eta(i) + \Delta t \times H_1(i) + \sqrt{\frac{2D \times \Delta t}{\tau^2}} \times R \right] / \tau}{2 + \left[\eta(i) + \Delta t \times H_1(i) + \sqrt{\frac{2D \times \Delta t}{\tau^2}} \times R \right]^2 \times (q-1) \times \beta}, \tag{15}$$

for $i = 1, 2, \dots$

2.3. Observables of interest

The stochastic motion of a test particle can be characterised in terms of the MSD. The latter can be calculated in terms of either an ensemble or a time average [20]. The ensemble-averaged MSD corresponds to the second moment about the origin of the PDF $P(x, t)$,

$$\langle x^2(t) \rangle = \int_{-\infty}^{\infty} x^2 P(x, t) dx, \tag{16}$$

where the angular brackets $\langle \cdot \rangle$ denote ensemble averages. For processes resulting in a power-law form $\langle x^2(t) \rangle \simeq K_\alpha t^\alpha$ with the generalised diffusion coefficient K_α , the anomalous diffusion exponent α allows one to distinguish subdiffusion ($0 < \alpha < 1$), normals diffusion ($\alpha = 1$), and superdiffusion ($\alpha > 1$) [20–22].

For an individual and sufficiently long trajectory, the time-averaged MSD (TAMSD) is

evaluated in terms of the sliding time average [20, 23]

$$\overline{\delta^2(\Delta)} = \frac{1}{T - \Delta} \int_0^{T-\Delta} [x(t + \Delta) - x(t)]^2 dt, \tag{17}$$

where T is the total measurement time (length) of the time series $x(t)$ and Δ is called the lag time. The overline $\overline{}$ denotes time averaging. The TAMSD compares the squared particle increments along the trajectory as separated by the time difference Δ , i.e., it corresponds to the squared deviations over a sliding window of width Δ . It is a function of both the lag time Δ and the length T of the time series, but we only indicate its Δ -dependence. To average out the fluctuations of individual TAMSDs $\overline{\delta_i^2(\Delta)}$ often the ensemble mean over N trajectories $x_i(t)$ is evaluated [20, 23, 145],

$$\langle \overline{\delta^2(\Delta)} \rangle = \frac{1}{N} \sum_{i=1}^N \overline{\delta_i^2(\Delta)}. \tag{18}$$

We call the stochastic process of interest ergodic (in the Boltzmann–Khinchin sense, which is looser than stricter ergodicity, e.g., in the mixing sense [146]) when we observe the long-time equivalence $\lim_{T \rightarrow \infty} \overline{\delta^2(t)} = \langle x^2(t) \rangle$. When this equivalence is not fulfilled we call the process (weakly) non-ergodic [20, 23, 145, 147]. Moreover, when the TAMSD explicitly depends on the measurement time T we call the process ageing [20, 23, 145, 147, 148]. While Brownian motion is ergodic, continuous time random walks with scale-free waiting times are (weakly) non-ergodic [20, 145, 147]. FBM is ergodic [147, 149] (note the transient non-ergodicity in confinement [40, 50]), while motion based on the generalised Langevin equation with a power law memory kernel is ergodic, except for the ballistic case [39, 40]. Experimental and simulation studies indeed unveiled such ergodicity breaking in heterogeneous media including cytoplasm and membranes of living cells [26, 29, 42, 51, 145].

For a given lag time Δ and finite T , the TAMSD varies from one trajectory to another, even for normal Brownian diffusion. The TAMSD therefore is a random variable. Defining the dimensionless variable $\zeta(\Delta) = \overline{\delta^2(\Delta)} / \langle \overline{\delta^2(\Delta)} \rangle$ the deviation of the amplitude of the TAMSD $\overline{\delta^2(\Delta)}$ of an individual trajectory with respect to the mean $\langle \overline{\delta^2(\Delta)} \rangle$ for a given lag time Δ can be quantified in terms of the PDF $\phi(\zeta)$ [20, 23, 145, 147]. The variance of this PDF is the ergodicity breaking parameter [20, 23, 145, 147, 150]

$$EB(\Delta) = \frac{\langle (\overline{\delta^2(\Delta)})^2 \rangle - \langle \overline{\delta^2(\Delta)} \rangle^2}{\langle \overline{\delta^2(\Delta)} \rangle^2} = \langle \zeta^2(\Delta) \rangle - 1. \tag{19}$$

Note that EB is often defined in the limit $T \rightarrow \infty$ for fixed Δ , and then (asymptotic) ergodicity is given for $\lim_{T \rightarrow \infty} EB = 0$. However, interesting information may be encoded in the explicit dependence on both Δ and T . For instance, for Brownian motion we obtain $EB = 4\Delta/(3T)$ [20, 23, 149]. Another measure for weak EB is the ratio of the mean TAMSD to the ensemble-average MSD [151]

$$\mathcal{EB}(\Delta) = \frac{\langle \overline{\delta^2(\Delta)} \rangle}{\langle x^2(\Delta) \rangle}. \tag{20}$$

3. Results and discussions

We now proceed to the analysis of the stochastic process given by equations (1) and (2), combining analytical calculations and simulations.

3.1. Theoretical approximations

For the analytical study we consider the system of stochastic equations

$$\frac{dx(t)}{dt} = \sqrt{2D_0|x|^\alpha}\eta(t), \tag{21}$$

$$\frac{d\eta(t)}{dt} = -\frac{1}{\tau} \frac{d}{d\eta} V_q(\eta) + \frac{1}{\tau} \xi(t), \tag{22}$$

in which we use the pure power-law $D_0|x|^\alpha$ for the position dependence of the diffusivity, and the exponent α is fixed or a random variable. The explicit form of $V_q(\eta)$ is given by equation (3). The state space variable of the system is (x, η) . The probability that the systems is in state (x, η) at time t is given by the single event PDF $P_q(x, \eta; t, \tau)$, that obeys the generalised ‘stochastic continuity equation’ (see appendix B)

$$\begin{aligned} \frac{\partial P_q(x, \eta; t, \tau)}{\partial t} = & -\frac{\partial}{\partial x} \left[\sqrt{2D_0|x|^\alpha}\eta P_q(x, \eta; t, \tau) \right] \\ & + \frac{\partial}{\partial \eta} \left[\left\langle \left(\frac{1}{\tau} \frac{d}{d\eta} V_q(\eta) - \frac{1}{\tau} \xi(t) \right) P_q(x, \eta; t, \tau) \right\rangle \right], \end{aligned} \tag{23}$$

subject to the initial condition $P_q(x, \eta; t = 0) = \delta((x, \eta) - (x_0, \eta_0))$. Recalling that the process $\eta(t)$ is driven by white Gaussian noise $\xi(t)$ given by equation (22), the PDF $P(\eta, t)$ is given by the average over the realisations of the stochastic driving force term $\xi(t)$,

$$P(\eta; t) = \langle \delta(\eta(t) - \eta) \rangle, \tag{24}$$

where the bracket $\langle \cdot \rangle$ means averaging with respect to the noise distribution. Note that $P_q(x, \eta; t, \tau) = P(x; t|\eta; t, \tau)P(\eta; t, \tau)$. Using (24) in the last part of (23), taking the average over all realisations of $\eta(t)$, and finally applying the law of total expectation, i.e., $\langle \xi(t)\delta(\eta(t) - \eta) \rangle = \langle \xi(t)\langle \delta(\eta(t) - \eta) | \xi(t) \rangle \rangle$ produces

$$\begin{aligned} \frac{\partial P_q(x, \eta; t, \tau)}{\partial t} = & -\sqrt{2D_0}\eta \frac{\partial}{\partial x} \left[\sqrt{|x|^\alpha} P_q(x, \eta; t, \tau) \right] \\ & + \frac{\partial}{\partial \eta} \left[\left(\frac{1}{\tau} \frac{d}{d\eta} V_q(\eta) \right) P_q(x, \eta; t, \tau) \right] \\ & - \frac{1}{\tau} \frac{\partial}{\partial \eta} \left[\langle \xi(t)\delta(\eta(t) - \eta) \rangle P(x; t|\eta; t, \tau) \right]. \end{aligned} \tag{25}$$

We recognise a correlation between the stochastic force $\xi(t)$ and its functional $\delta(\eta(t) - \eta)$. The average in the last term of equation (25) can be evaluated via Novikov’s theorem. For the Gaussian white noise $\xi(t)$ with zero mean the noise noise functional is given as

$$\begin{aligned} \langle \xi(t)\delta(\eta(t) - \eta) \rangle = & \int_0^t dt' \gamma(t, t') \left\langle \frac{\delta[\delta(\eta(t) - \eta)]}{\delta \xi(t')} \right\rangle, \\ = & -\frac{\partial}{\partial \eta} \int_0^t dt' \gamma(t, t') \left\langle \delta(\eta(t) - \eta) \frac{\delta \eta(t)}{\delta \xi(t')} \right\rangle, \end{aligned} \tag{26}$$

where $\gamma(t, t') = \langle \xi(t)\xi(t') \rangle = 2D\delta(t - t')$, and where the quantity $\delta\eta(t)/\delta\xi(t')$ is a functional derivative of $\eta(t)$ with respect to $\xi(t')$. The latter may be interpreted as the non-averaged response function of $\eta(t)$ to the stochastic force $\xi(t')$. Substituting (26) into (25) yields

$$\begin{aligned} \frac{\partial P_q(x, \eta; t, \tau)}{\partial t} &= -\sqrt{2D_0} \frac{\partial}{\partial x} \left[\sqrt{|x|^\alpha} \eta P_q(x, \eta; t, \tau) \right] \\ &+ \frac{\partial}{\partial \eta} \left[\frac{1}{\tau} \frac{d}{d\eta} V_q(\eta) \right] P_q(x, \eta; t, \tau) \\ &+ \frac{D}{\tau} \frac{\partial}{\partial \eta} \left\{ \left[\frac{\partial}{\partial \eta} \int_0^t dt' \delta(t - t') \right. \right. \\ &\times \left. \left. \left\langle \delta(\eta(t) - \eta) \frac{\delta\eta(t)}{\delta\xi(t')} \right\rangle \right] P(x; t|\eta; t, \tau) \right\}. \end{aligned} \quad (27)$$

The functional derivative $\delta\eta(t)/\delta\xi(t')$ is evaluated by first performing a formal time integration of the second equation in (21),

$$\eta(t) = -\frac{1}{\tau} \int_0^t ds \frac{d}{d\eta} V_q(\eta(s)) + \frac{1}{\tau} \int_0^t ds \xi(s). \quad (28)$$

Here we used $\eta(t = 0) = 0$. Then taking the functional derivative with respect to $\xi(t')$ yields

$$\begin{aligned} \frac{\delta\eta(t)}{\delta\xi(t')} &= -\frac{1}{\tau} \int_{t'}^t ds \frac{\delta \left[\frac{d}{d\eta} V_q(\eta(s)) \right]}{\delta\xi(t')} + \frac{1}{\tau} \int_{t'}^t ds \frac{\delta\xi(s)}{\delta\xi(t')}, \\ &= -\frac{1}{\tau} \int_{t'}^t ds \frac{\delta \left[\frac{d}{d\eta} V_q(\eta(s)) \right]}{\delta\xi(t')} + \frac{1}{\tau}. \end{aligned} \quad (29)$$

The lower integration limit is due to causality meaning $t' \leq s$.

For convenience take $\delta\eta(t)/\delta\xi(t') \approx \frac{1}{\tau}$ which is justified by considering the approximation given in equation (31). Thus, the FPE for the PDF $P_q(x, \eta; t, \tau)$ is finally given as

$$\begin{aligned} \frac{\partial P_q(x, \eta; t, \tau)}{\partial t} &= -\sqrt{2D_0} \eta \frac{\partial}{\partial x} \left[\sqrt{|x|^\alpha} P_q(x, \eta; t, \tau) \right] \\ &+ \frac{\partial}{\partial \eta} \left[\left(\frac{1}{\tau} \frac{d}{d\eta} V_q(\eta) \right) P_q(x, \eta; t, \tau) \right] \\ &+ \frac{D}{\tau^2} \frac{\partial^2}{\partial \eta^2} P_q(x, \eta; t, \tau). \end{aligned} \quad (30)$$

For simplicity and tractability of the computation, η^2 in $dV_q(\eta)/d\eta$ can be approximated by its expectation, i.e., $\eta^2 \approx \langle \eta^2 \rangle = 2D/[\tau(5 - 3q)]$ [140, 152, 153]. Thus,

$$\frac{d}{d\eta} V_q(\eta) = \eta \left[1 + \frac{\beta}{2}(q - 1)\langle \eta^2 \rangle \right]^{-1} \approx \eta \left[\frac{2(2 - q)}{5 - 3q} \right]^{-1} = \frac{\eta}{r_q}, \quad (31)$$

where $r_q = 2(2 - q)/(5 - 3q)$. With this approximation the coloured non-Gaussian noise process (2) can be rewritten as an Ornstein–Uhlenbeck process,

$$\frac{d\eta(t)}{dt} = -\frac{\eta}{\tau_q} + \frac{r_q}{\tau_q} \xi(t), \quad (32)$$

with the correlation time $\tau_q = \tau r_q$ and the noise intensity r_q . Using the approximation (31) in the FPE (30) leads us to

$$\begin{aligned} \frac{\partial P_q(x, \eta; t, \tau)}{\partial t} &= -\sqrt{2D_0}\eta \frac{\partial}{\partial x} \left\{ \sqrt{|x|^\alpha} P_q(x, \eta; t, \tau) \right\} \\ &+ \frac{1}{\tau_q} \frac{\partial}{\partial \eta} \{ \eta P_q(x, \eta; t, \tau) \} + \frac{r_q^2 D}{\tau_q^2} \frac{\partial^2}{\partial \eta^2} P_q(x, \eta; t, \tau). \end{aligned} \quad (33)$$

3.1.1. Method of moments approach. We now use the method of moments approach to coloured noise in order to obtain an effective stochastic differential equation. The $[m, n]$ th joint moment of $[x, \eta]$ about the origin is defined by

$$\langle x^m \eta^n \rangle = \int dx \int d\eta x^m \eta^n P_q(x, \eta; t), \quad (34)$$

where m and n are integers. Multiplying equation (33) by $x^m \eta^n$, then integrating with respect to x and η yields the evolution equation for the joint moments $\langle x^m \eta^n \rangle$. Setting m and n appropriately we have

$$\frac{d\langle x \rangle}{dt} = \sqrt{2D_0} \langle \eta |x|^{\frac{\alpha}{2}} \rangle, \quad (35a)$$

$$\frac{d\langle \eta \rangle}{dt} = -\frac{1}{r_q \tau} \langle \eta \rangle, \quad (35b)$$

$$\frac{d\langle x^2(t) \rangle}{dt} = 2\sqrt{2D_0} \langle \eta x |x|^{\frac{\alpha}{2}} \rangle, \quad (35c)$$

$$\frac{d\langle \eta^2 \rangle}{dt} = -\frac{2}{r_q \tau} \langle \eta^2 \rangle + \frac{2D}{\tau^2}, \quad (35d)$$

$$\frac{d\langle x\eta \rangle}{dt} = \sqrt{2D_0} \langle \eta^2 |x|^{\frac{\alpha}{2}} \rangle - \frac{1}{r_q \tau} \langle x\eta \rangle. \quad (35e)$$

We now define the quantities $\mu_x, \nu, \gamma, \zeta,$ and χ corresponding to means and (co)variances,

$$\mu_x = \langle x \rangle, \quad (36a)$$

$$\nu = \langle \eta \rangle, \quad (36b)$$

$$\gamma = \langle x^2 \rangle - \langle x \rangle^2, \quad (36c)$$

$$\zeta = \langle \eta^2 \rangle - \langle \eta \rangle^2, \quad (36d)$$

$$\chi = \langle x\eta \rangle - \langle x \rangle \langle \eta \rangle. \quad (36e)$$

The evolution equations for these quantities can be derived by first expanding equations (35a) to (35e) with $x = \mu_x + \delta x$ and $\eta = \nu + \delta \eta$ around their mean values and retaining terms up to the order of $\langle (\delta x)^2 \rangle$. Assuming that $\langle \delta x \rangle = 0$ and $\langle \delta \eta \rangle = 0$, we see that $\gamma = \langle (\delta x)^2 \rangle, \zeta = \langle (\delta \eta)^2 \rangle,$ and $\chi = \langle \delta x \delta \eta \rangle$. We then get

$$\frac{d\mu_x}{dt} = \sqrt{2D_0} \left(\nu |\mu_x|^{\frac{\alpha}{2}} + \frac{1}{2} \frac{\alpha(\alpha-2)}{2} \nu |\mu_x|^{\frac{(\alpha-4)}{2}} \gamma + \frac{\alpha}{2} |\mu_x|^{\frac{(\alpha-2)}{2}} \chi \text{sign}(\mu_x) \right), \quad (37a)$$

$$\frac{d\nu}{dt} = -\frac{\nu}{r_q\tau}, \tag{37b}$$

$$\frac{d\gamma}{dt} = 2\sqrt{2D_0} \left(|\mu_x|^{\frac{\alpha}{2}} \chi + \frac{\alpha}{2} \nu |\mu_x|^{\frac{(\alpha-2)}{2}} \gamma \operatorname{sign}(\mu) \right), \tag{37c}$$

$$\frac{d\zeta}{dt} = -\frac{2}{r_q\tau} \zeta + \frac{2D}{\tau^2}, \tag{37d}$$

$$\frac{d\chi}{dt} = \sqrt{2D_0} \left(|\mu_x|^{\frac{\alpha}{2}} \zeta + \frac{\alpha}{2} \nu |\mu_x|^{\frac{(\alpha-2)}{2}} \chi \operatorname{sign}(\mu_x) \right) - \frac{1}{r_q\tau} \chi. \tag{37e}$$

The stationary values are given by

$$\nu_s = 0, \tag{38a}$$

$$\zeta_s = \frac{D}{\tau} r_q, \tag{38b}$$

$$\chi_s = \frac{\sqrt{2D_0} D r_q^2 |\mu_x|^{\frac{\alpha}{2}}}{\left(1 - \alpha \tau_q \sqrt{\frac{D_0}{2}} v |\mu|^{\frac{\alpha-2}{2}} \operatorname{sign}(\mu) \right)}. \tag{38c}$$

Using equations (38a)–(38c) in (37a) and (37c), the evolution equation for the mean μ and variance γ becomes

$$\frac{d\mu_x}{dt} = \sqrt{2D_0} v |\mu|^{\frac{\alpha-4}{2}} \left[|\mu|^2 + \frac{1}{2} \frac{\alpha}{2} \left(\frac{\alpha-2}{2} \right) \frac{D r_q^2}{\tau_q} \right] + \frac{\alpha D_0 D r_q^2}{|\mu|^{\frac{\alpha}{2}} \left(|\mu|^{\frac{\alpha}{2}} \operatorname{sign}(\mu) - \alpha \tau_q \sqrt{\frac{D_0}{2}} v \right)}, \tag{39a}$$

$$\frac{d\gamma}{dt} = \frac{4D_0 D r_q^2 |\mu|^\alpha}{\left(1 - \alpha \tau_q \sqrt{\frac{D_0}{2}} v |\mu|^{\frac{\alpha-2}{2}} \operatorname{sign}(\mu) \right)} + \alpha \sqrt{2D_0} v |\mu|^{\frac{\alpha-2}{2}} \gamma \operatorname{sign}(\mu). \tag{39b}$$

Notice that the factor $D r_q^2$ in equations (39a) and (39b) depends on the coloured non-Gaussian noise. When $\alpha = 0$, corresponding to homogeneous diffusion with non-Gaussian noise, equations (39a) and (39b) simplify substantially.

We now define the effective diffusion coefficient

$$\begin{aligned} D_{\text{eff}} &= \frac{2r_q \sqrt{D_0 D} |x|^\alpha}{\sqrt{\left(1 - \tau_q \frac{\alpha}{2} \sqrt{2D_0} \eta |x|^{\frac{\alpha-2}{2}} \operatorname{sign}(x) \right)}} \\ &= \sqrt{\frac{8D_0 D r_q^2 |x|^{\alpha+1}}{\left(2|x| - \alpha \tau_q (dx/dt) \operatorname{sign}(x) \right)}}. \end{aligned} \tag{40}$$

The coefficient D_{eff} depends on q , D , and τ , the parameters q -noise, as well as the scaling exponent α . The effective stochastic differential equation for x may be then expressed as

$$\frac{dx}{dt} = D_{\text{eff}} \xi(t), \tag{41}$$

where $\xi(t)$ is Gaussian white noise with zero mean and delta noise correlation $2D\delta(t - t')$. For $q = 1$ equation (41) corresponds to the original HDP process with Gaussian white driving noise. Squaring equation (41) and setting $(dx(t)/dt)^2 = 0$ yields the ordinary differential equation

$$\frac{dx}{dt} = \frac{2|x|}{\alpha\tau_q \text{sign}(x)} (1 - 4D_0Dr_q^2|x|^\alpha). \tag{42}$$

Now setting $d^2x/dt^2 = 0$, D_{eff} is written as

$$\begin{aligned} D_{\text{eff}} &= \sqrt{\frac{4D_0Dr_q^2|x|^\alpha}{1 - r_q\sqrt{2D_0}\left(1 + \frac{2|x|}{\alpha\tau_q}\right)^{-1}|x|^{\alpha/2} \text{sign}(x)\xi(t)}} \\ &= \sqrt{4D_0Dr_q^2|x|^\alpha} \sum_{n=0}^{\infty} \frac{1}{2^{2n}} \binom{2n}{n} \\ &\quad \times \left[r_q\sqrt{2D_0}\left(1 + \frac{2|x|}{\alpha\tau_q}\right)^{-1} |x|^{\alpha/2} \text{sign}(x)\xi(t) \right]^n. \end{aligned} \tag{43}$$

Retaining only terms up to first order in $\xi(t)$ equation (41) becomes

$$\frac{dx}{dt} = \sqrt{4D_0Dr_q^2|x|^\alpha} \xi(t). \tag{44}$$

As a consequence of this truncation the effect of the parameter τ is lost, which implies that the noise correlation time does not affect the long time behaviour, as it should. The FPE of the PDF $P_q(x, t)$ corresponding to equation (44) reads

$$\frac{\partial P_q(x, t)}{\partial t} = 4D_0D_qr_q^2 \frac{\partial}{\partial x} \left\{ |x|^{\alpha/2} \frac{\partial}{\partial x} (|x|^{\alpha/2} P_q(x, t)) \right\}, \tag{45}$$

with $D_q = 2D^2$. For $\alpha = 0$, we have

$$P_q(x, t) = \frac{1}{\sqrt{8\pi D_0D_qr_q^2t}} \exp\left(-\frac{x^2}{8D_0D_qr_q^2t}\right), \tag{46}$$

which is a Gaussian PDF with mean zero and variance $2^3D_0[D([2 - q]/[5 - 3q])]^2t$. In this case the ensemble averaged MSD is equal to the variance which means it is linear in time. More generally, the solution of equation (45) is derived by applying the procedure used in [88], leading to (see appendix A)

$$P_q(x, t) = \frac{|x|^{1/p-1}}{\sqrt{8\pi D_0D_qr_q^2t}} \exp\left(-\frac{|x|^{2/p}}{2(2/p)^2D_0D_qr_q^2t}\right). \tag{47}$$

Here $p = 2/(2 - \alpha)$ and $D_q = 2D^2$. The ensemble averaged MSD is given as

$$\langle x^2(t) \rangle = \frac{\Gamma(p + \frac{1}{2})}{\sqrt{\pi}} \left[\sqrt{D_0D_q} \frac{2}{p} \left(\frac{2 - q}{5 - 3q} \right) \right]^{2p} t^p. \tag{48}$$

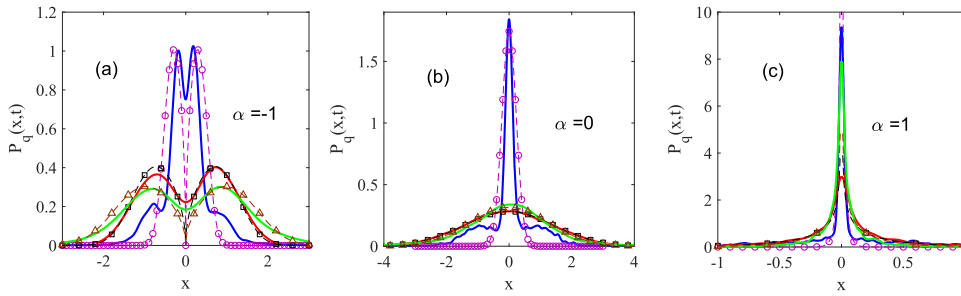


Figure 1. Theoretical PDFs according to equation (47) (dashed lines with symbols) and simulations results (solid lines) for $D_0 = 0.01$, $D = 0.5$, $\tau = 1$, and for various q values ($q = 0.1$: purple dashed line with circles and full blue line; $q = 1$: black dashed line with squares and red line; $q = 1.5$: orange dashed line with triangles and full green line). In the different panels, the diffusivity scaling exponent is (a) $\alpha = -1$, (b) $\alpha = 0$, and (c) $\alpha = 1$. The initial position in all cases is at the origin. In panel (a) $t = 3, 25$, and 15 for $q = 0.1, 1.0$, and 1.5 . In panel (b) $t = 4, 100$, and 20 for $q = 0.1, 1.0$, and 1.5 . In panel (c) $t = 5, 50$, and 8 for $q = 0.1, 1.0$, and 1.5 .

For $q = 1$ and $D = 1$ equations (47) and (48) are similar to the corresponding ones for the standard HDP process with Gaussian noise found in [88]. The only difference arises from the definition of the delta-correlation of the noise. Whereas in [88] $\langle \xi(t)\xi(t') \rangle = \delta(t - t')$ (the noise strength there was solely taken to be represented by D_0) in our case it is $2D\delta(t - t')$. The scaling of the ensemble MSD in equation (48), i.e., $\langle x^2(t) \rangle \sim t^\nu$ implies subdiffusion for $-2 < \alpha < 0$, normal diffusion for $\alpha = 0$, and superdiffusion for $0 < \alpha$. The special case $\alpha = 1$ is ballistic motion, and sometimes the case $1 < \alpha < 2$ is called hyperdiffusion. It should be noted that our approximation may lead to loss of information of the transient dynamics in the theoretical model. To capture the complete behaviour we use numerical simulations.

Figure 1 compares the analytical PDF (47) to the simulations results. Generally, the theoretical and the simulated results show good agreement. We note that the simulations are based on the regularised law (4) for the position dependence of the diffusion coefficient while the analytical form (47) is based on the pure power-law with $a = 0$. Therefore smaller deviations are observed especially around the origin. Analogously to the results in the original investigation in [88] the distribution is bimodal and dips to zero at $x = 0$ for $\alpha = -1$; it is bell-shaped for $\alpha = 0$, while for $\alpha = 1$ the curves are inverted funnel-shaped with a cusp at $x = 0$. For both $\alpha = -1$ and 0 , the PDFs have larger peaks but are less stretched for $q = 0.1$, whereas they have smaller peaks but are more stretched for $q = 1.5$. For $\alpha = 1$ the PDF for $q = 0.1$ has a larger peak and is more stretched while for $q = 1.5$ it has a smaller peak and is less stretched. The shapes reflect the degree of non-Gaussianity of the noise amplitude as well as the precise form of $D(x)$, the latter implying higher diffusivity away from the origin for $\alpha > 0$ and vice versa. Generally the shapes of the PDF indicate that the particles become enriched in zones of smaller diffusivity. Thus both α and q affects the shape of the distribution around the origin and in the tails.

Figure 2 shows the PDF on a log-linear scale for different non-extensivity parameter q and scaling exponents α at time $t = 2$. The PDF broadens with increasing q , i.e., particle spreading is enhanced for larger q . The tails broaden with increasing α , and vice versa. The solid green line with squares ($q = 1$ and $\alpha = 0$) corresponds to the Gaussian case, i.e., the limiting case of normal Gaussian diffusion.

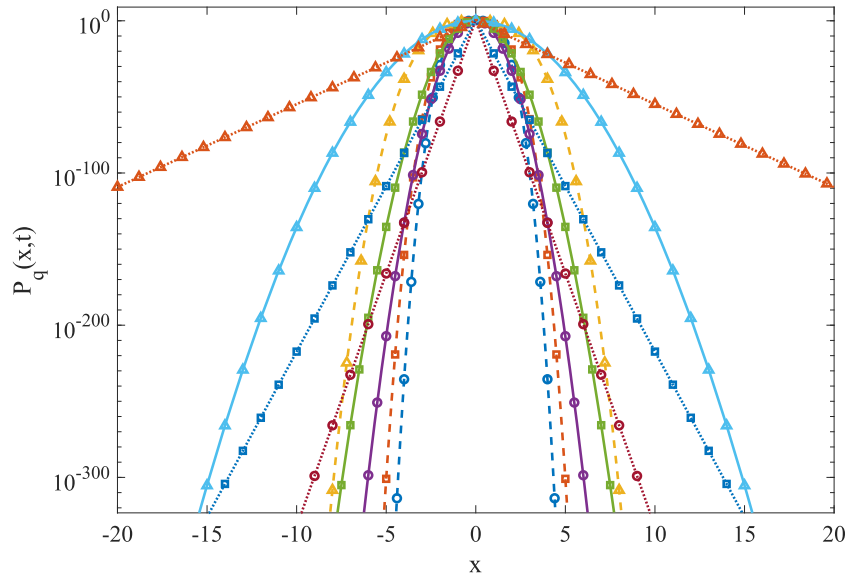


Figure 2. PDF according to equation (47) for various q and α . The dashed, solid and dotted lines are for $\alpha = -1, 0,$ and $1,$ respectively. The circles, squares, and triangles represent $q = 0.1, 1.0,$ and $1.5,$ respectively. We chose $D = 0.5, D_0 = 0.01,$ and $t = 2.0.$

3.2. Simulations results

We now proceed to discuss the results of our simulations in more detail. We first consider the case of an unstratified medium, in which the diffusion coefficient varies according to equation (4) on the entire x -axis. In the second part we consider a stratified medium in which equidistant slices are each governed by a law of the type (4).

3.2.1. Unstratified medium. In this subsection simulation results are presented for the situation that the diffusivity changes over the entire range $x \in (-\infty, \infty).$ The quantities we evaluate are the ensemble- and TAMSD, the EB parameters, and the non-Gaussian parameter.

Ensemble and TAMSD. Figure 3 presents the TAMSD for 1000 individual trajectories along with the mean TAMSD and the ensemble averaged when the correlation time is short, here, $\tau = 1.$ The non-extensivity parameter q is varied horizontally across the figure as $q = 0.1, 1.0,$ and $1.5,$ while the diffusivity scaling exponent α is varied vertically, as $\alpha = -1, 0,$ and $1.$ The case of $\alpha = 0,$ when the diffusion coefficient is constant ($= D_0$), corresponds to diffusion in an homogeneous medium, otherwise the medium is heterogeneous with a position-varying diffusion coefficient. The other parameters for all panels are $D = 0.5$ and $D_0 = 0.1,$ and the initial position is uniformly distributed between -1 and $1.$ The overall analysed time of each trajectory is $T = 10^4.$ The curves of the individual TAMSD are almost parallel and close to each other in panel (a). In (d) and (g) the trajectories are also almost parallel but are more scattered. In (e) the trajectories coincide for shorter lag times, implying almost perfect reproducibility from one trajectory to another, but at longer lag times significant scatter emerges. Conversely in panels (b), (c), (f), (h), and (i) the trajectories are scattered for all lag times. Due to decreasing statistic the scatter is generally more pronounced for longer lag times.

In all panels the trajectories nicely follow the trend set by the mean TAMSD (blue solid curve). They show superdiffusive scaling at shorter lag times, that is, Δ^γ with $\gamma = 1.5$ in (b),

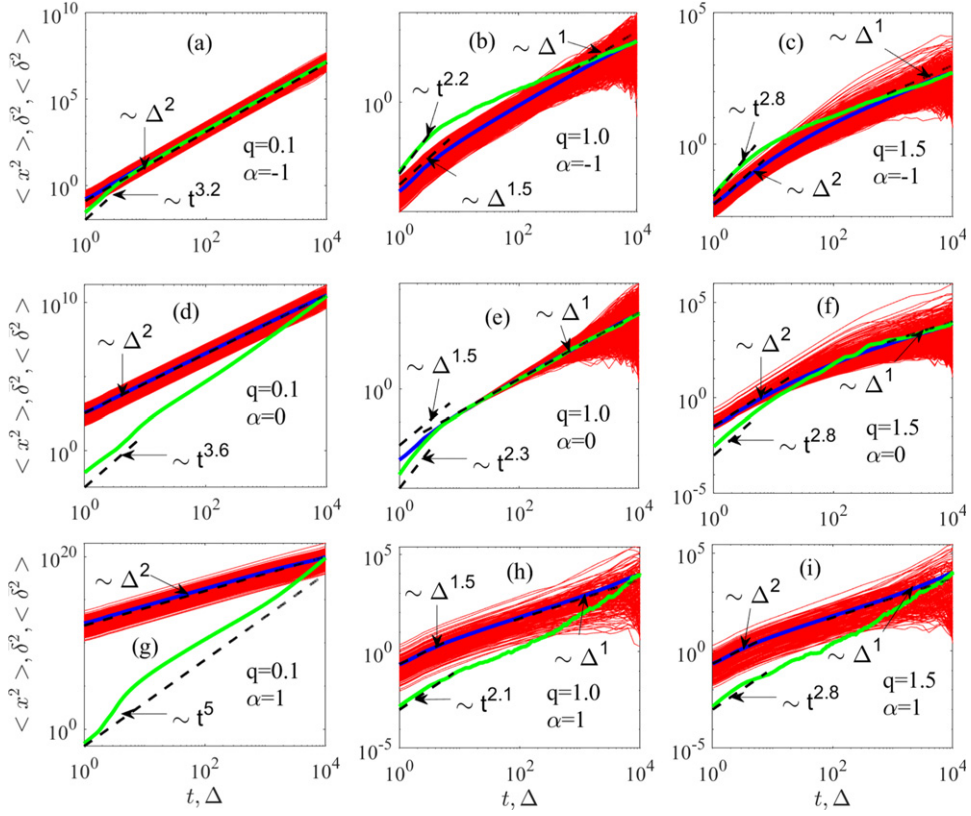


Figure 3. Ensemble averaged MSD (green curves), TAMSD (red curves) of 1000 individual trajectories, and mean TAMSD (blue curves) with $q = 0.1$ in (a), (d), and (g); $q = 1.0$ in (b), (e), and (h); $q = 1.5$ in (c), (f), and (i). We chose $\alpha = 0$ in (a)–(c); $\alpha = -1$ in (d)–(f); $\alpha = 1$ in (g)–(i). Other parameters: $\tau = 1$, $D = 0.5$, $D_0 = 0.01$. The total measurement time for the TAMSD is $T = 10^4$.

(e) and (h) $q = 1.0$; and ballistic motion with $\gamma = 2$ for $q = 0.1$ and 1.5 . At longer lag times the mean TAMSD exhibits ballistic motion ($\gamma = 2$) for $q = 0.1$ and normal diffusion ($\gamma = 1$) for $q = 1.0$ and 1.5 , respectively. Notice that for $q = 0.1$ the scaling of the ensemble averaged TAMSD suggests ballistic motion at all lag times whereas for $q = 1.0$ and 1.5 it displays a crossover from ballistic to normal diffusion.

The ensemble averaged MSD shows a scaling of the form $\langle x^2(t) \rangle \simeq t^{2+\lambda}$ with $0.1 \leq \lambda \leq 3$, which implies hyperdiffusion at shorter and intermediate times, before coinciding with the mean TAMSD at longer times. The two quantities are almost coinciding in panels (a), (e), and (f) even for shorter lag times, a signature of ergodic behaviour. In contrast, in panels (d), (g)–(i) the ensemble averaged MSD is much smaller than the mean TAMSD at short time scales. In panels (b) and (c) it is larger. At longer time scales the ensemble averaged MSD and the mean TAMSD converge in all panels. The disparity between the ensemble averaged MSD and the mean TAMSD at shorter lag times indicates a (transient) weak ergodicity breaking.

The scaling exponent λ of the ensemble averaged MSD $\langle x^2(t) \rangle \simeq t^{2+\lambda}$ ranging in the interval $0 < \lambda < 3$ has been reported in tracer particles in turbulent flows [154] and tilted washboard potentials [39]. For a short correlation time, the long time power-law scaling is $\langle x^2(t) \rangle \sim t^p$

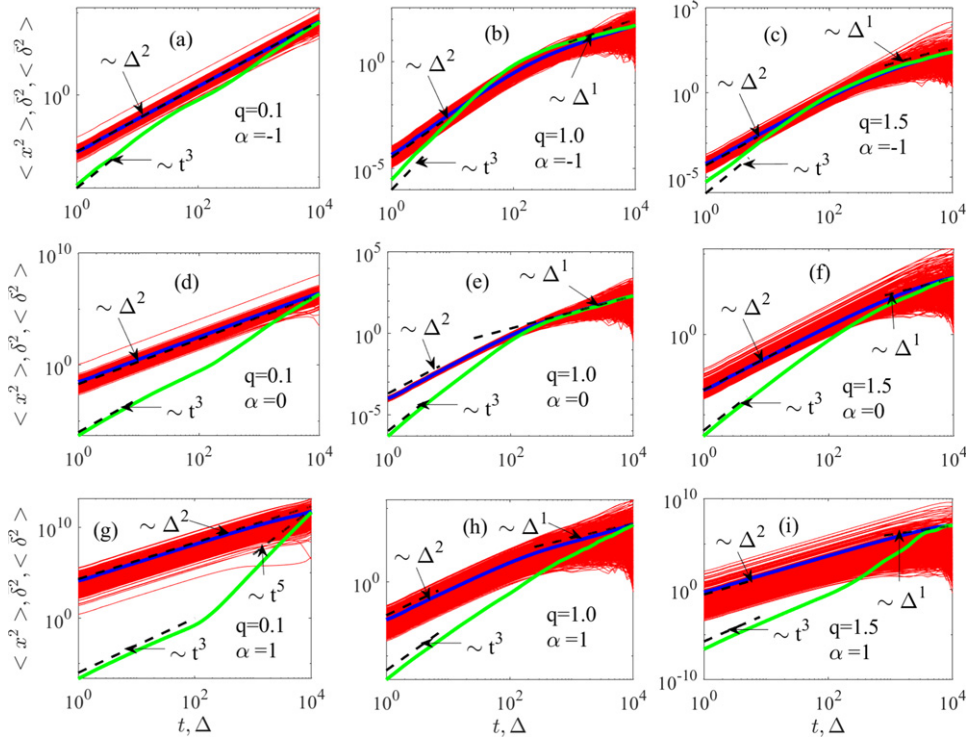


Figure 4. TAMSD (red curves) from 1000 individual trajectories; ensemble averaged MSD (green curves); and average TAMSD (blue curves), with $q = 0.1$ in (a), (d), and (g); $q = 1.0$ in (b), (e), and (h); $q = 1.5$ in (c), (f), and (i). We have $\alpha = 0$ in (a)–(c); $\alpha = -1$ in (d)–(f); $\alpha = 1$ in (g)–(i). Other parameters: $\tau = 100$, $D = 0.5$, and $D_0 = 0.01$. The total measurement time is $T = 10^4$.

where $p = \frac{2}{2-\alpha}$ according to equation (48) (see the original derivation in [88]) holds when $q = 1$; this case corresponds to panels (b), (e), and (f). The fact that equation (48) predicts the same scaling exponent p also for non-Gaussian noise with $q \neq 1$ is shown for $q = 1.5$ in panels (c), (f), and (i); for $q = 0.1$ the correct scaling is also seen in panel (g), while for panels (a) and (d) the crossover to this scaling occurs at later times.

Figure 4 presents simulation results for the TAMSD, mean TAMSD, and the ensemble averaged MSD for the case of a long correlation time, i.e., $\tau = 100$. In all panels the individual TAMSD trajectories are somewhat scattered which indicates a high degree of irreproducibility of the TAMSD. Naturally the scatter becomes more pronounced at longer lag times. The TAMSD curves follow the trend given by the mean TAMSD. At shorter lag times the ensemble averaged TAMSD and the mean MSD show a significant disparity, i.e., weak ergodicity breaking. Whereas the scaling of the ensemble averaged TAMSD implies ballistic motion, $\simeq \Delta^2$, the scaling of the ensemble averaged MSD suggests hyper-diffusion, $t^{2+\lambda}$ with $\lambda = 1$ or 1.2 . At longer lag times, however, the two averaged quantities coincide. The scaling suggests ballistic motion for $q = 0.1$, i.e., in panels (a), (d), and (g); superdiffusion in panel (h); standard diffusion in panels (e), (f), and (i); and subdiffusion in panels (b) and (c). The theoretical power-law exponent of the ensemble averaged MSD, equation (48), holds in panels (b), (c), (e)–(g), while the convergence has not occurred in the other panels (check this statement).

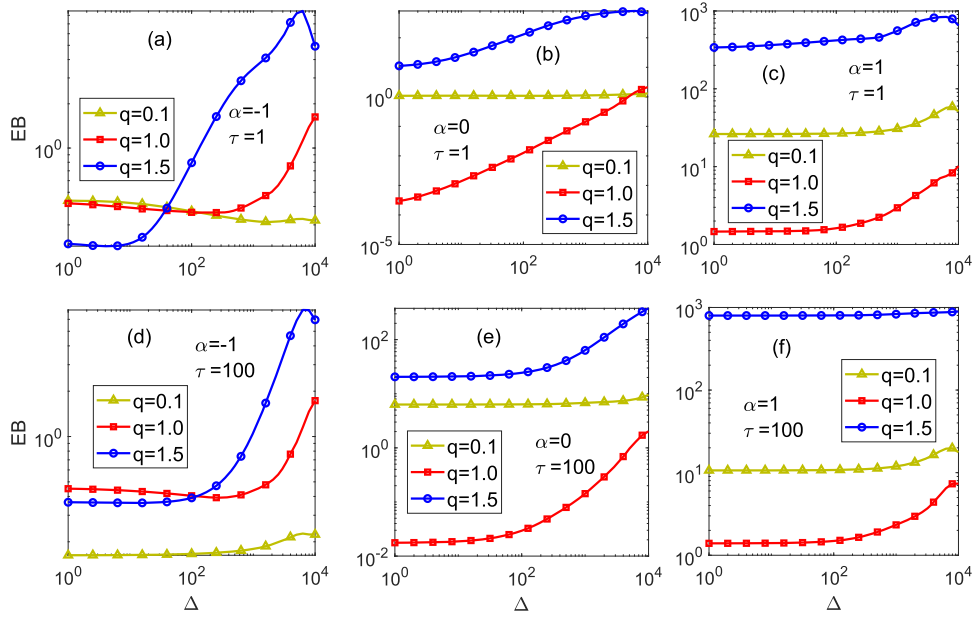


Figure 5. Ergodicity breaking parameter EB as function of lag time Δ for varying non-extensivity index q . In (a) and (d) $\alpha = -1$; in (b) and (e) $\alpha = 0$; in (c) and (f) $\alpha = 1$. Moreover, $\tau = 1$ in (a)–(c); $\tau = 100$ in (d)–(f). Parameters: $D = 0.5$, $D_0 = 0.01$, and $T = 10^4$.

EB parameters. We now turn to the ergodicity breaking parameters EB and \mathcal{EB} , quantifying, respectively, the variance of the amplitude fluctuations of individual TAMSD curves and the relative deviation from ergodicity.

Figure 5 shows the dependence of the ergodicity breaking parameter EB on the lag time Δ . In all panels, EB is non-zero for all lag times. For $\Delta \ll T$, EB converges to a plateau, whose value strongly depends on the non-extensivity index q . As $\Delta \rightarrow T$, EB increases with growing Δ for $q = 1.0$ and 1.5 , except in panel (f) where it remains constant for $q = 1.5$. For $q = 0.1$ EB remains fairly constant with a small growth in panels (c), (d), and (f), and a small decrease in panel (a) at very long lag times. When $\alpha = -1$, EB assumes small values at short lag times and larger values at longer lag times, except for $q = 0.1$, for which it is small at all lag times. When $\alpha = 0$ EB assumes small values for $q = 1.0$ and large values for $q = 0.1$ and $q = 1.5$. EB is small and large, respectively, for $\tau = 1$ and $\tau = 100$. Conversely, for $\alpha = 1$ EB assumes large values for all three q values. Generally, statistically reliable information is obtained at shorter lag times, when $\Delta \ll T$. Notice that for $\alpha = 0$, $q = 1.0$, and $\tau = 1$, EB is close to zero when $\Delta \ll T$ and then grows as $\frac{\Delta}{T}$, which is consistent with the behaviour of EB for standard Brownian motion in homogeneous media. We find that as $\frac{\Delta}{T} \rightarrow 0$ EB is very close to zero when $q = 1$ and $\alpha = 0$ for both $\tau = 1$ and 100 , indicating ergodic behaviour. In all other panels EB assumes non-negligible values, indicating significant fluctuations among individual trajectories.

Figure 6 shows the dependence of the ergodicity breaking parameter EB on the trace length T . The value $EB(\Delta = 1)$ for the case $q = 1.0$ and $\alpha = 0$ matches that of Brownian motion ($EB = (4/3)\Delta/T$) while in all other cases it is significantly greater. EB also varies with q .

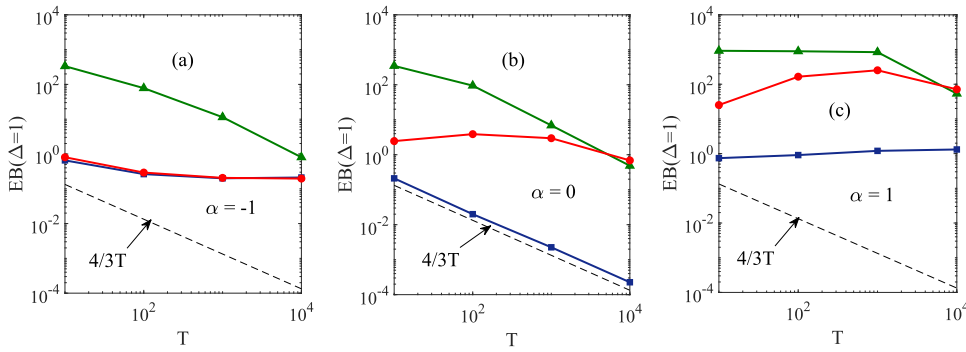


Figure 6. Dependence of the ergodicity breaking parameter $EB(\Delta = 1)$ on the total trace time T for different values of the non-extensivity parameter q and the diffusivity scaling exponent α . The solid lines with symbols of triangle, square, and circle are for $q = 0.1, 1.0,$ and $1.5,$ respectively. The dashed line stands for Brownian motion. Parameters: $\tau = 1, D_0 = 0.01,$ and $D = 0.5$.

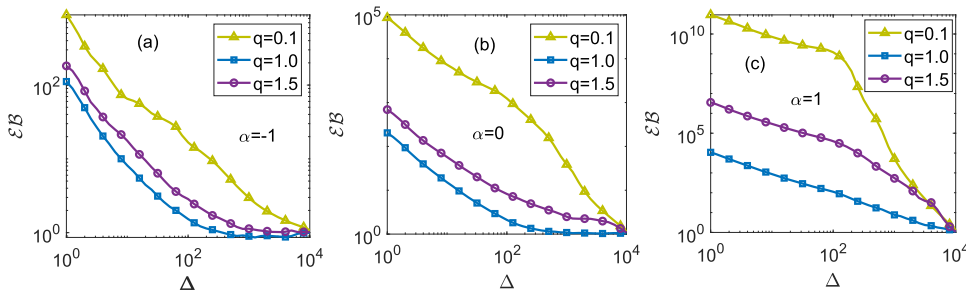


Figure 7. Ergodicity breaking parameter \mathcal{EB} as function of the lag time Δ for varying q , and with $\alpha = -1, 0$ and 1 in (a)–(c), respectively. Parameters: $\tau = 100, D = 0.5, D_0 = 0.01,$ and $T = 10^4$.

Generally, it decreases as $T \rightarrow \infty$, except for the case when $q = 1.0$ and $\alpha = 1$, for which it remains almost constant close to one. Both q and α lead to deviations from Brownian motion.

Figure 7 displays the dependence of the ergodicity breaking parameter \mathcal{EB} on lag time Δ for different q with $\tau = 100$. In all panels \mathcal{EB} is significantly greater than one for $\Delta \ll T$ whereas it approaches unity as $\Delta \rightarrow T$. It assumes higher values for $q = 0.1$ and lower ones for $q = 1.0$. It decreases rapidly to one, representing the fact that in the weakly divergent case $\Delta \rightarrow T$ the mean TAMSD coincides with the ensemble averaged MSD. Although the curves show the same overall trend they exhibit variations for different q and α indicating that \mathcal{EB} is affected by both parameters, as expected. For the ergodic system in the sense of the MSDs, $\mathcal{EB} = 1$.

Non-Gaussianity parameter. The non-Gaussianity parameter is an indicator for a deviation of the displacement PDF from a Gaussian. A systematic analysis of the non-Gaussianity of a process may provide clues for the origin of the anomalous behaviour. It is defined as the ratio of the fourth moment of the TAMSD versus the squared second moment. In one dimension it

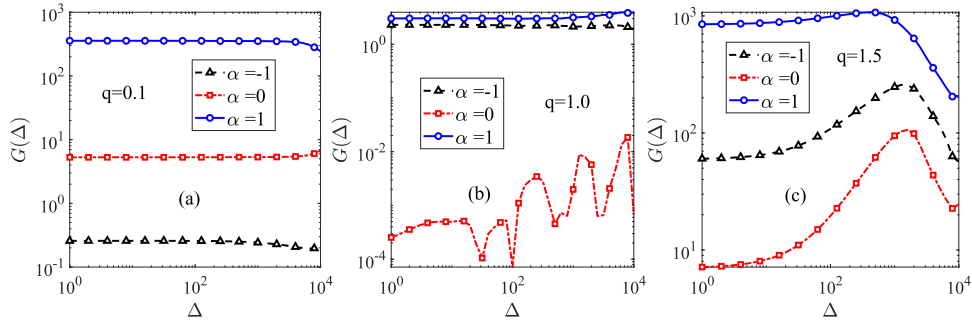


Figure 8. Non-Gaussian parameter G as function of lag time Δ for varying diffusivity scaling exponent α . We show results for the non-extensivity parameter $q = 0.1, 1.0,$ and 1.5 in panels (a)–(c), respectively. Parameters: $\tau = 10, D = 0.5,$ and $D_0 = 0.01$.

is given by

$$G(\Delta) = \frac{1}{3} \frac{\langle \overline{\delta^4(\Delta)} \rangle}{\langle \overline{\delta^2(\Delta)} \rangle^2} - 1, \quad (49)$$

where we define

$$\langle \overline{\delta^4(\Delta)} \rangle = \frac{1}{T - \Delta} \int_0^{T-\Delta} (x(t + \Delta) - x(t))^4 dt. \quad (50)$$

A $G(\Delta)$ value close to zero implies Gaussian statistics whereas values significantly greater than zero indicate more heterogeneous diffusion dynamics. Here we show the non-Gaussianity as function of the lag time Δ and the non-extensivity parameter q .

Figure 8 examines the behaviour of $G(\Delta)$ for varying α with q fixed. When $q = 0.1$ in panel (a), $G(\Delta)$ assumes small, moderate, and large values for $\alpha = -1, 0,$ and $1,$ respectively. It remains constant at short and medium lag times but gradually grows for $\alpha = 0$ or descends for $\alpha = -1$ and 1 as $\Delta \rightarrow T$. When $q = 1.0$ in panel (b), $G(\Delta)$ is very close to zero for $\alpha = 0$ and close to one for $\alpha = -1$ and 1 . In the former case, it is constant for short lag times but grows at long lag times. Conversely, in the latter case it remains constant at all lag times. When $q = 1.5$ in panel (c), $G(\Delta)$ assumes moderately large values for $\alpha = 0$ but substantially larger values for $\alpha = -1$ and 1 in the range of short lag times. In both cases it remains approximately constant. In the range of longer lag times $G(\Delta)$ assumes larger values. It first grows, then descends for $\alpha = 0$ and $\alpha = -1,$ while it descends for $\alpha = 1$. When $q = 1.0$ and $\alpha = 0$ the process is Gaussian and homogeneous, and $G(\Delta)$ has practically zero value. All other cases yield substantially larger values for the non-Gaussian parameter implying significant deviations from Gaussian behaviour, as expected. For a fixed α the curves of $G(\Delta)$ for different q show varying behaviours implying that q affects $G(\Delta),$ another expected effect albeit we could not find explicit analytical expressions for the detailed behaviour. We emphasise the existence of a pronounced maximum of the non-Gaussianity for the case $q = 1.5$.

3.2.2. Stratified medium. Consider now the situation in which the medium is divided into strata (layers). In a given stratum of width $2\delta x$ the scaling exponent α of the diffusivity is constant and $D(x)$ is centred symmetrically around the mid-point of the stratum. Across strata

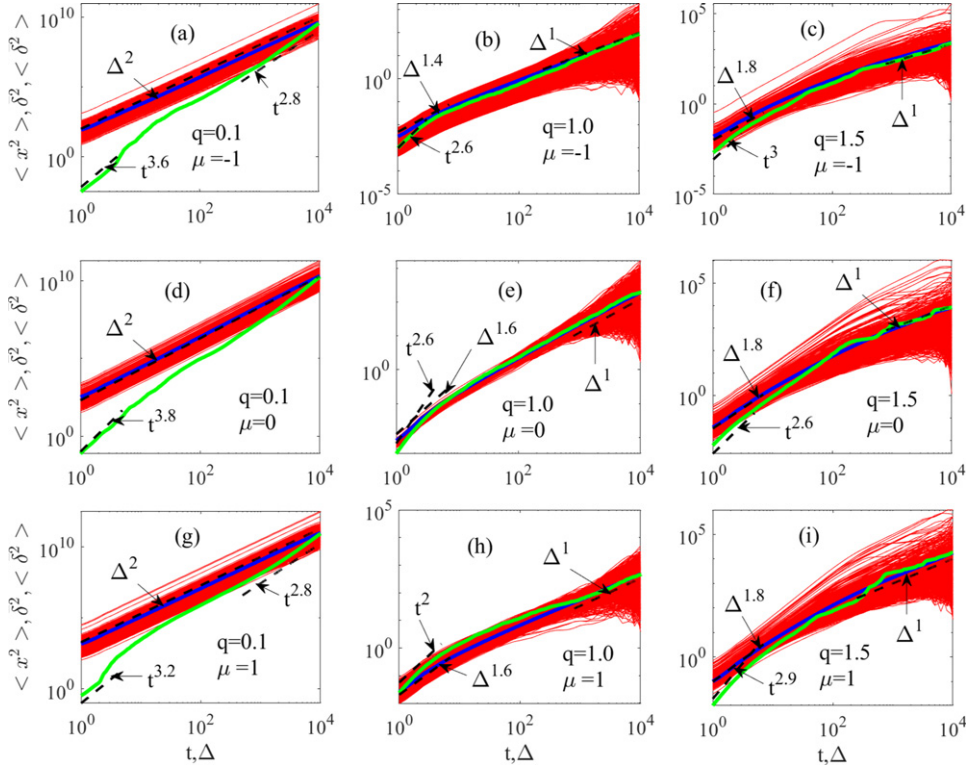


Figure 9. TAMSD (red curves) from 1000 individual trajectories, ensemble mean TAMSD (blue curves), and averaged MSD (green curves), with $q = 0.1$ in (a), (d), and (g); $q = 1.0$ in (b), (e), and (h); $q = 1.5$ in (c), (f), and (i). We chose $\mu = 0$ in (a)–(c); $\mu = -1$ in (d)–(f); $\mu = 1$ in (g)–(i). Parameters: $\sigma = 1$, $\delta x = 10$, $\tau = 1$, $D = 0.5$, and $D_0 = 0.01$. The total measurement time is $T = 10^4$.

α is normally distributed with mean μ and standard deviation σ , as previously considered in the white Gaussian-noise scenario of [114].

TAMSD, ensemble averaged TAMSD and MSD. Figure 9 shows the TAMSD for individual trajectories, the mean TAMSD, and the ensemble averaged MSD when the correlation time is short, i.e., $\tau = 1$. The non-extensivity parameter q and the mean μ of the diffusivity scaling exponent are varied in the panels across and vertically, respectively. For $q = 0.1$ the individual TAMSD trajectories are almost parallel and equally scattered at all lag times. In all other panels the trajectories are scattered, more pronounced at longer lag times. In the left panels, i.e., for $q = 0.1$ there is a significant disparity between the ensemble averaged MSD and the mean TAMSD at both shorter and longer lag times. At shorter lag times the mean TAMSD exhibits ballistic motion ($\sim \Delta^2$), while the ensemble averaged MSD shows hyperdiffusive scaling, i.e., $t^{2+\lambda}$ with $\lambda = 1.6, 1.8$, and 1.2 in panels (a), (d), and (g), respectively. In the centre and the right panels, at $\Delta \ll T$ the ensemble averaged MSD exhibits hyperdiffusive scaling $t^{2+\lambda}$ with $\lambda = 0.6$ in panels (b), (e), and (f); 1 and 0.9 in panels (c) and (i), respectively. It displays ballistic motion in panel (h). Concurrently the ensemble average TAMSD shows superdiffusive scaling Δ^γ with $\gamma = 1.4$ in panel (b), 1.6 in panels (e) and (h), and 1.8 in panels (c), (f), and (i). At longer lag times the mean TAMSD and the ensemble averaged MSD coincide. Panels (a), (d), and (g) indicate ballistic motion while all other panels show normal diffusion. The disparity

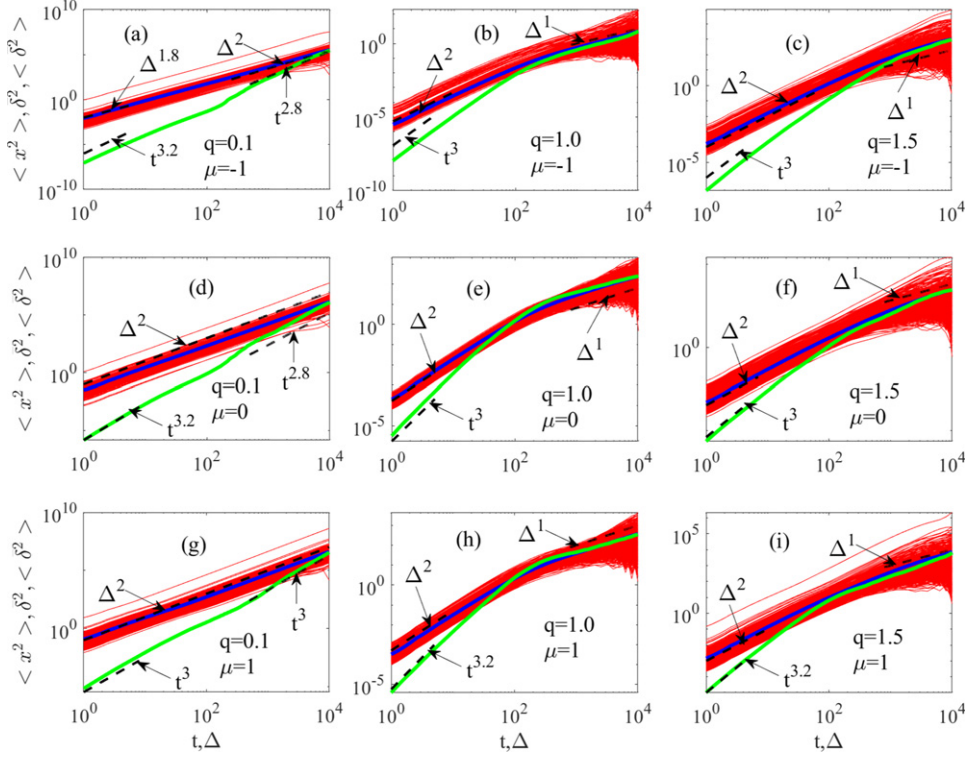


Figure 10. TAMSD (red curves) from 1000 individual trajectories, mean TAMSD (blue curves), and ensemble averaged MSD (green curves), with $q = 0.1$ in (a), (d), and (g); $q = 1.0$ in (b), (e), and (h); $q = 1.5$ in (c), (f), and (i). We chose $\mu = 0$ in (a)–(c); $\mu = -1$ in (d)–(f); $\mu = 1$ in (g)–(i). Parameters: $\sigma = 1$, $\delta x = 10$, $\tau = 100$, $D = 0.5$, and $D_0 = 0.01$. The total measurement time is $T = 10^4$.

between the mean TAMSD and the ensemble averaged MSD for $\Delta \ll T$ is a signature of weak non-ergodicity.

Figure 10 shows the TAMSD, the mean TAMSD, and the ensemble averaged MSD for long correlation time, $\tau = 100$. In panels (a), (d), and (g), i.e., for $q = 0.1$, the curves for the TAMSD are almost parallel and scattered at all lag times. In all other panels the TAMSD curves form a band that broadens for longer lag times. The amplitude scatter is more pronounced at longer lag times. Generally, the TAMSD curves follow the trend given by their mean. In panel (a) the mean TAMSD scales as $\Delta^{1.8}$ at short lag times and as Δ^2 at longer lag times, i.e., we observe superdiffusion and ballistic motion, respectively. In all other panels the scaling of the mean TAMSD at shorter lag times is ballistic, $\simeq \Delta^2$. At longer lag times the scaling is still ballistic in panels (d) and (g), while in panels (b), (c), (e), (f), (h), and (i) the scaling is $\simeq \Delta$, i.e., normal diffusive. In all panels the ensemble averaged MSD exhibits hyperdiffusive scaling $\simeq t^{2+\lambda}$ with $\lambda = 1$ in panels (b), (c), (e)–(g); and with $\lambda = 1.2$ in panels (a), (d), (h), and (i). At short times the ensemble averaged MSD and the mean TAMSD are disparate, respectively with hyperdiffusive and ballistic scaling. At long times the two quantities coincide. The degree of disparity is large for $q = 0.1$ and for $\mu = -1$. The deviations between the mean TAMSD and ensemble averaged MSD at $\Delta \ll T$ is more pronounced in figure 10, i.e., when $\tau = 100$ than in figure 9, when $\tau = 1$, which implies that the ergodicity depends on the noise correlation time.

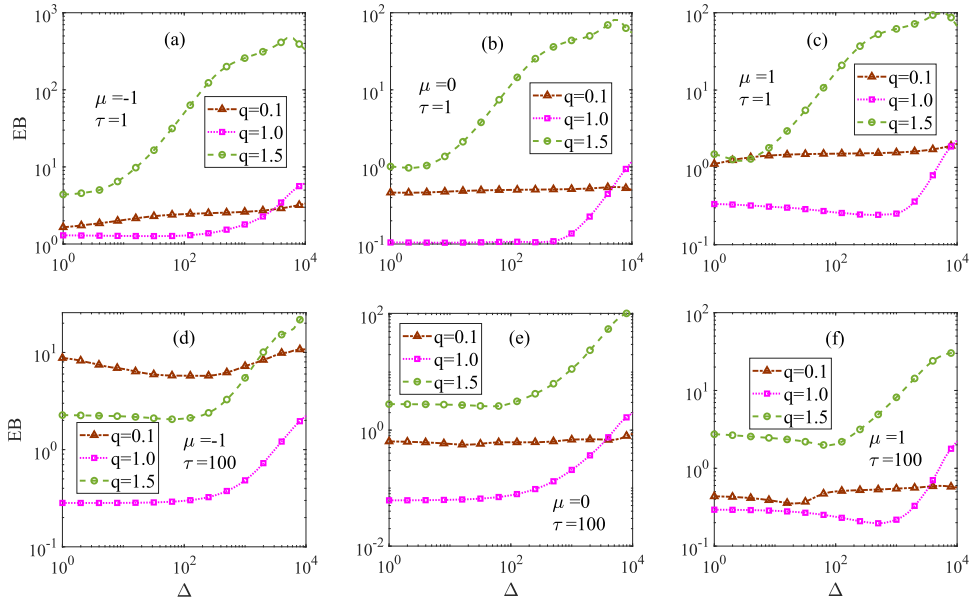


Figure 11. Ergodicity breaking parameter EB as function of lag time Δ for varying non-extensivity parameter q . In (a) and (d), $\mu = -1$; in (b) and (e), $\mu = 0$; in (c) and (f), $\mu = 1$. Parameters: $\tau = 1$ in (a)–(c); $\tau = 100$ in (d)–(f). In all panels $\sigma = 1$, $\delta x = 10$, $D = 0.5$, $D_0 = 0.01$, and $T = 10^4$.

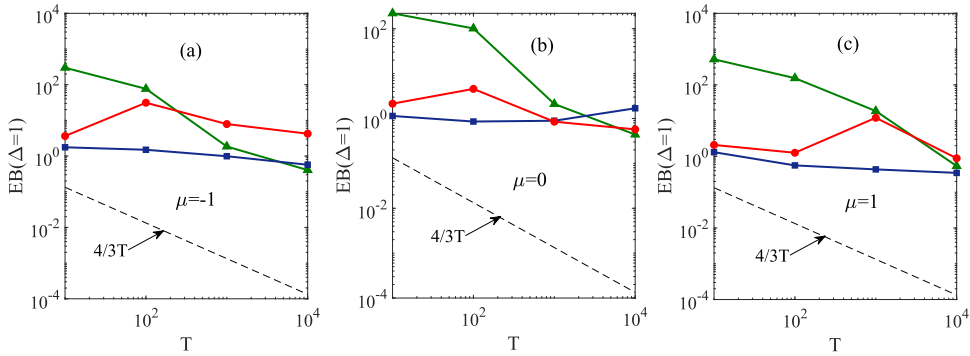


Figure 12. Dependence of the ergodicity breaking parameter $EB(\Delta = 1)$ on the trace length T . In all panels, the solid lines with triangle, square, and circle are for $q = 0.1$, 1.0 , and 1.5 , respectively. The dashed line represents Brownian motion. The diffusivity scaling exponent α varies across the panels while $\sigma = 1$, $\tau = 1$, $\delta x = 10$, $D = 0.5$, and $D_0 = 0.01$ are fixed.

EB parameters. We now turn to the ergodicity breaking parameters EB and \mathcal{EB} . Figure 11 shows the dependence of EB on lag time. EB assumes small values at all lag times for $q = 0.1$ and 1.0 , while for $q = 1.5$ it exhibits small values for shorter lag times, i.e., $\tau \ll T$ and large values for longer lag times. For $q = 0.1$ it remains constant at all lag times whereas for $q = 1.0$ and 1.5 it is constant at shorter lag times but grows steadily with increasing lag time for longer

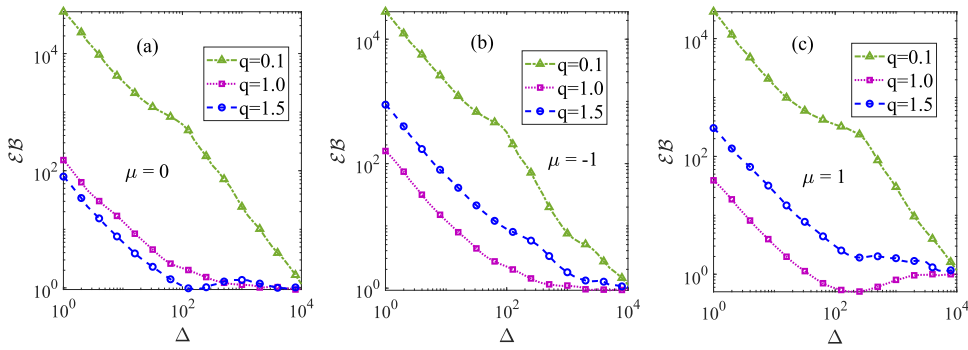


Figure 13. Ergodicity breaking parameter \mathcal{EB} as function of time lag Δ for varying q , and with $\mu = 0, -1$, and 1 in (a)–(c), respectively. We chose $\sigma = 1, \delta x = 10, \tau = 100, D = 0.5, D_0 = 0.01$, and $T = 10^4$.

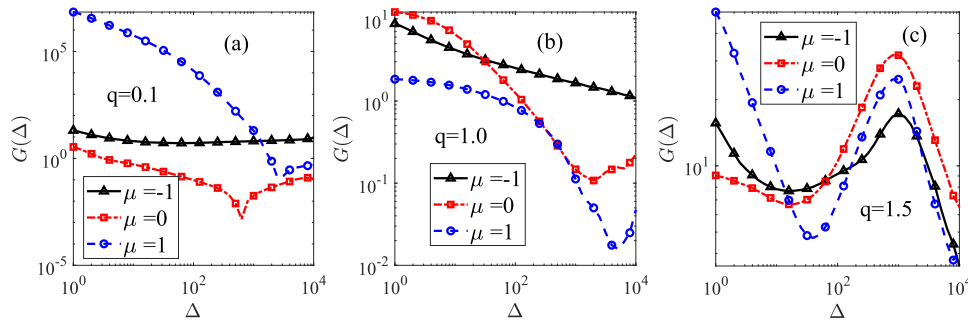


Figure 14. Non Gaussianity parameter G as function of Δ for varying μ . We chose $q = 0.1, 1.0$, and 1.5 in panels (a)–(c), respectively. Parameters: $\sigma = 1, \delta x = 10, \tau = 10, D = 0.5$, and $D_0 = 0.01$.

lag times. In all panels EB is smallest for $q = 1.0$ at shorter lag times, while at longer lag times crossings between the lines for different q are observed.

Figure 12 shows a significant deviation of the ergodicity breaking parameter $\mathcal{EB}(\Delta = 1)$ from the behaviour of Brownian motion. Whereas the behaviour is the same for all μ , it varies with the non-extensivity index q . As $T \rightarrow \infty$, $\mathcal{EB}(\Delta = 1)$ decreases.

Figure 13 shows the dependence of \mathcal{EB} on lag time for varying q . For $\Delta \ll T$, \mathcal{EB} assumes larger values and decreases with increasing lag time. It flattens at some intermediate lag times, then decreases again for $q = 0.1$ or increases gradually for $q = 1.0$ and $q = 1.5$, and approaches unity as $\Delta \rightarrow T$. For each q , \mathcal{EB} exhibits a similar trend for $\mu = 0, -1$, and 1 .

Non-Gaussian parameter. Figure 14 presents the non-Gaussian parameter as a function of lag time for varying μ . For $q = 0.1$ panel (a), $G(\Delta)$ decreases with increasing Δ at short and intermediate lag times but flattens as $\Delta \rightarrow T$ for $\mu = 0$ and 1 ; for $\mu = -1$ it remains constant at all lag times. For $q = 1.0$ in panel (b), $G(\Delta)$ descends linearly with lag time for $\mu = -1$, while for $\mu = 0$ and 1 it descends and ascends in the short and long lag time regimes, respectively. For $q = 1.5$ in panel (c), $G(\Delta)$ is decreasing, increasing, and then decreasing again at shorter, intermediate, and longer lag times, respectively. For a given μ , the curves of $G(\Delta)$ vary with q .

4. Conclusions

We studied the diffusive motion of a test particle experiencing a spatially varying diffusion coefficient while driven by coloured non-Gaussian noise, a relevant scenario in a variety of physical and biological systems. Concretely, the noise is distributed according to Tsallis' q -distribution and follows an Ornstein–Uhlenbeck process, i.e., it is exponentially correlated. In particular, this means that the generated noise is stationary. We used the TAMSD, the mean TAMSD, and the ensemble averaged MSD to quantify the emerging anomalous diffusion dynamics. The process is further analysed in terms of the EB parameters and the non-Gaussian parameter. We considered unstratified and stratified media.

We showed that the non-extensivity parameter q affects the effective diffusivity but not the scaling exponent of the ensemble averaged MSD. The non-Gaussianity of the emerging PDFs depend on both q and the scaling exponent α of the diffusivity. Depending on q , α , and the noise correlation time τ , individual TAMSD traces can be widely scattered, implying a significant degree of irreproducibility for large parameter ranges. Both the mean TAMSD and the ensemble averaged MSD reveal several diffusion regimes. The ensemble averaged MSD exhibits hyperdiffusion at shorter times, ballistic motion and superdiffusion at intermediate times, and standard or subdiffusion at longer times. The mean TAMSD shows ballistic motion, superdiffusion, or normal diffusion at shorter times; superdiffusion or normal diffusion at intermediate times; and normal or subdiffusion at longer times. For short noise correlation time, the mean TAMSD and the ensemble averaged MSD coincide for $\alpha = 0$ and $q = 1$, indicating ergodic behaviour (at times longer than τ effective Brownian motion emerges) but they differ for the other cases in the short lag time regime, implying significant weak ergodicity breaking. For long noise correlation time, the mean TAMSD and MSD exhibit significant disparity on the analysed time scales.

The ergodicity breaking parameters EB and \mathcal{EB} depend on q , α , and τ . Depending on whether the medium is unstratified or stratified, EB exhibits striking behaviours as function of lag time or measurement time, including minima and maxima at intermediate times. Lacking fully analytic solutions this behaviour was analysed in detail from simulations. For short noise correlation times, EB indicates ergodicity breaking in both media. However, it is close to zero for $q = 0.1$ in a stratified medium, implying almost vanishing non-ergodicity. As expected, it corresponds to the behaviour for homogeneous diffusion for $q = 1.0$ and $\alpha = 0$. The non-Gaussianity parameter $G(\Delta)$ also depends markedly on the parameters q and α .

The coloured non-Gaussian heterogeneous diffusion model introduced here provides a highly flexible model to capture complex stochastic motion in heterogeneous media. While we unveiled several interesting features here, the detailed behaviour of the ergodic behaviour of this model will be explored in more detail in future work.

Acknowledgments

This work was supported by the NSF of China (Grants No. 11772255 No. 11902118), the National Key Research and Development Program of China under Grant No. 2018AAA0102201, the Research Funds for Interdisciplinary Subject of Northwestern Polytechnical University, the Shaanxi Project for Distinguished Young Scholars, the Shaanxi Provincial Key R & D Program 2020KW-013 and 2019TD-010. RM acknowledges financial support from the German Research Foundation (DFG), Grant No. ME 1535/12-1 as well as from the Foundation for Polish Science (Fundacja na rzecz Nauki Polskiej, FNP) within an Alexander von Humboldt Honorary Polish Research Scholarship. We also thank Aggrey Adem for helpful discussions.

Data availability statement

No new data were created or analysed in this study.

Appendix A. Probability density function

Here, we provide the key steps to solve the Langevin equation (44) in the Stratonovich sense applying the procedure used in [88]. Introduce the substitution

$$y(x) = \int^x \frac{dx'}{\sqrt{4D_0Dr_q^2|x'|^\alpha}},$$

which implies that

$$\frac{dy}{dx} = \frac{1}{\sqrt{4D_0Dr_q^2|x|^\alpha}}.$$

Using the chain rule, $\frac{dy}{dt} = \frac{dy}{dx} \frac{dx}{dt}$, we find that

$$\dot{y}(t) = \xi(t),$$

with $\langle \xi(t)\xi(t') \rangle = 2D\delta(t - t')$, that is, a Brownian process for which the PDF of y is Gaussian with mean zero and variance $2Dt$. For initial condition $y(0) = 0$, the PDF becomes

$$P(y, t) = \frac{1}{\sqrt{4\pi Dt}} \exp\left(-\frac{y^2}{4Dt}\right).$$

Our aim is to obtain the PDF of the random variable x . To that end we first define y explicitly in terms of x

$$y = \frac{1}{\sqrt{4D_0Dr_q^2}} \int^x |x'|^{-\frac{\alpha}{2}} dx' = \frac{1}{\sqrt{4D_0Dr_q^2}} \frac{|x|^{\frac{1}{p}}}{\frac{1}{p}} \text{sign}(x),$$

with $p = 2/(2 - \alpha)$. Thus,

$$\frac{dy}{dx} = \frac{|x|^{1/p-1}}{\sqrt{4D_0Dr_q^2}},$$

and then the PDF of x yields in the form

$$P_q(x, t) = \frac{|x|^{1/p-1}}{\sqrt{8\pi D_0D_qr_q^2t}} \exp\left\{-\frac{|x|^{2/p}}{2(2/p)^2 D_0D_qr_q^2t}\right\},$$

with $D_q = 2D^2$.

Appendix B. The stochastic continuity equation

We here provide some details on the derivation of the stochastic continuity equation (23). Starting with the stochastic equations (21) and (22) consider (x, η) to be a vector in (two-dimensional) phase space. Let $P_q(x, \eta; t, \tau)$ represent the density of the system at point (x, η) and time t , where (x, η) is the solution of the above systems such that $(x, \eta, t = 0) = (x_0, \eta_0)$. Then $P_q(x, \eta; t, \tau)$ can be expressed in terms of an average over realisations of the noise $\xi(t)$,

$$P_q(x, \eta; t, \tau) = \langle \delta((x, \eta) - (x_0, \eta_0)) \rangle,$$

which satisfies the ‘stochastic continuity equation’

$$\frac{\partial P_q(x, \eta; t, \tau)}{\partial t} + \frac{\partial \{ \dot{x} P_q(x, \eta; t, \tau) \}}{\partial x} + \frac{\partial \{ \dot{\eta} P_q(x, \eta; t, \tau) \}}{\partial \eta} = 0,$$

subject to the initial condition

$$P_q(x, \eta; t = 0) = \delta((x, \eta) - (x_0, \eta_0)).$$

Substituting $\dot{x}(t)$ and $\dot{\eta}(t)$ yields the sought-after relation (23). Here, the brackets $\langle \cdot \rangle$ denotes averaging over realisations of the noise $\xi(t)$.

ORCID iDs

Yong Xu  <https://orcid.org/0000-0002-8407-4650>

Ralf Metzler  <https://orcid.org/0000-0002-6013-7020>

References

- [1] Einstein A 1905 Über die von der molekularkinetischen Theorie der Wärme geforderte Bewegung von in ruhenden Flüssigkeiten suspendierten Teilchen *Ann. Phys.* **322** 549
- [2] von Smoluchowski M 1906 Zur kinetischen Theorie der Brownschen Molekularbewegung und der Suspensionen *Ann. Phys.* **326** 756
- [3] Brown R 1828 XXVII. A brief account of microscopical observations made in the months of June, July and August 1827, on the particles contained in the pollen of plants; and on the general existence of active molecules in organic and inorganic bodies *Phil. Mag.* **4** 161
- [4] Zwanzig R 2001 *Nonequilibrium Statistical Mechanics* (Oxford: Oxford University Press)
- [5] Landau L D and Lifshitz E M 1999 *Physical Kinetics* (Oxford: Heinemann)
- [6] Brenig W 1989 *Statistical Theory of Heat: Nonequilibrium Phenomena* (Berlin: Springer)
- [7] Langevin P 1908 Sur la théorie du mouvement brownien *C. R. Acad. Sci., Paris* **146** 530
- [8] van Kampen N G 1981 *Stochastic Processes in Physics and Chemistry* (Amsterdam: North-Holland)
- [9] Hughes B D 1995 *Random Walks and Random Environments, Vol 1: Random Walks* (Oxford: Oxford University Press)
- [10] von Hippel P H and Berg O G 1989 Facilitated target location in biological systems *J. Biol. Chem.* **264** 675
- [11] Pulkkinen O and Metzler R 2013 Distance matters: the impact of gene proximity in bacterial gene regulation *Phys. Rev. Lett.* **110** 198101
- [12] Godec A and Metzler R 2016 Universal proximity effect in target search kinetics in the few encounter limit *Phys. Rev. X* **6** 041037
- [13] Spagnolo B and Valenti D 2008 Volatility effects on the escape time in financial market models *Int. J. Bifurcation Chaos* **18** 2775

- [14] Giuffrida A, Valenti D, Ziino G, Spagnolo B and Panebianco A 2009 A stochastic interspecific competition model to predict the behaviour of *Listeria monocytogenes* in the fermentation process of a traditional Sicilian salami *Eur. Food Res. Technol.* **228** 767
- [15] Gelhar L W and Axness C L 1983 Three-dimensional stochastic analysis of macrodispersion in aquifers *Water Resour. Res.* **19** 161
- [16] Richardson L F 1926 Atmospheric diffusion shown on a distance-neighbour graph *Proc. R. Soc. A* **110** 709
- [17] Scher H and Montroll E W 1975 Anomalous transit-time dispersion in amorphous solids *Phys. Rev. B* **12** 2455
- [18] Scher H, Shlesinger M F and Bendler J T 1991 Time-scale invariance in transport and relaxation *Phys. Today* **44** 26
- [19] Klafter J, Shlesinger M F and Zumofen G 1996 Beyond Brownian motion *Phys. Today* **49** 33
- [20] Barkai E, Garini Y and Metzler R 2012 Strange kinetics of single molecules in living cells *Phys. Today* **65** 29
- [21] Bouchaud J-P and Georges A 1990 Anomalous diffusion in disordered media: statistical mechanisms, models and physical applications *Phys. Rep.* **195** 127
- [22] Metzler R and Klafter J 2000 The random walk's guide to anomalous diffusion: a fractional dynamics approach *Phys. Rep.* **339** 1
- [23] Metzler R, Jeon J-H, Cherstvy A G and Barkai E 2014 Anomalous diffusion models and their properties: non-stationarity, non-ergodicity, and ageing at the centenary of single particle tracking *Phys. Chem. Chem. Phys.* **16** 24128
- [24] Höfling F and Franosch T 2013 Anomalous transport in the crowded world of biological cells *Rep. Prog. Phys.* **76** 046602
- [25] Norregaard K, Metzler R, Ritter C M, Berg-Sørensen K and Oddershede L B 2017 Manipulation and motion of organelles and single molecules in living cells *Chem. Rev.* **117** 4342
- [26] Metzler R, Jeon J-H and Cherstvy A G 2016 Non-Brownian diffusion in lipid membranes: experiments and simulations *Biochim. Biophys. Acta Biomembr.* **1858** 2451
- [27] Golding I and Cox E C 2006 Physical nature of bacterial cytoplasm *Phys. Rev. Lett.* **96** 098102
- [28] Weber S C, Spakowitz A J and Theriot J A 2010 *Phys. Rev. Lett.* **104** 238102
- [29] Jeon J-H *et al* 2011 *In vivo* anomalous diffusion and weak ergodicity breaking of lipid granules *Phys. Rev. Lett.* **106** 048103
- [30] Bronstein I, Israel Y, Kepten E, Mai S, Shav-Tal Y, Barkai E and Garini Y 2009 *Phys. Rev. Lett.* **103** 018102
- [31] Schuille P, Happts U, Maiti S and Webb W W 1999 *Biophys. J.* **77** 2251
- [32] Jeon J-H, Monne H M, Javanainen M and Metzler R 2012 *Phys. Rev. Lett.* **109** 188103
- [33] Goepfert N, Goldscheider N and Berkowitz B 2020 Experimental and modeling evidence of kilometer-scale anomalous tracer transport in an alpine karst aquifer *Water Res.* **178** 115755
- [34] Dentz M, Le Borgne T, Englert A and Bijeljic B 2011 Mixing, spreading and reaction in heterogeneous media: a brief review *J. Contam. Hydrol.* **120–121** 1
- [35] Caspi A, Granek R and Elbaum M 2001 Enhanced diffusion in active intracellular transport *Phys. Rev. Lett.* **85** 5655
- [36] Arcizet D, Meier B, Sackmann E, Rädler J and Heinrich D 2009 Temporal analysis of active and passive transport in living cells *Phys. Rev. Lett.* **101** 248103
- [37] Reverey J F, Jeon J-H, Leippe M, Metzler R and Selhuber-Unkel C 2015 *Sci. Rep.* **5** 11690
- [38] Song M S, Moon H C, Jeon J-H and Park H Y 2018 Neuronal messenger ribonucleoprotein transport follows an aging Lévy walk *Nat. Commun.* **9** 344
- [39] Siegle P, Goychuk I and Hänggi P 2010 Origin of hyperdiffusion in generalized Brownian motion *Phys. Rev. Lett.* **105** 100602
- [40] Jeon J-H and Metzler R 2012 Inequivalence of time and ensemble averages in ergodic systems: exponential versus power-law relaxation in confinement *Phys. Rev. E* **85** 021147
- [41] Klafter J, Blumen A and Shlesinger M F 1987 Stochastic pathway to anomalous diffusion *Phys. Rev. A* **35** 3081
- [42] Weigel A V, Simon B, Tamkun M M and Krapf D 2011 Ergodic and nonergodic processes coexist in the plasma membrane as observed by single-molecule tracking *Proc. Natl Acad. Sci.* **108** 6438
- [43] Mandelbrot B B and van Ness J W 1968 Fractional Brownian motions, fractional noises and applications *SIAM Rev.* **10** 422

- [44] Pei B, Xu Y and Yin G 2018 Averaging principles for SPDEs driven by fractional Brownian motions with random delays modulated by two-time-scale Markov switching processes *Stoch. Dyn.* **18** 1850023
- [45] Pei B, Xu Y, Yin G and Zhang X 2018 Averaging principles for functional stochastic partial differential equations driven by a fractional Brownian motion modulated by two-time-scale Markovian switching processes *Nonlinear Anal. Hybrid Syst.* **27** 107
- [46] Mei R, Xu Y and Kurths J 2019 Transport and escape in a deformable channel driven by fractional Gaussian noise *Phys. Rev. E* **100** 022114
- [47] Pei B, Xu Y and Wu J-L 2020 Stochastic averaging for stochastic differential equations driven by fractional Brownian motion and standard Brownian motion *Appl. Math. Lett.* **100** 106006
- [48] Pei B, Xu Y, Xu Y and Bai Y 2020 Convergence of p th mean in an averaging principle for stochastic partial differential equations driven by fractional Brownian motion *Discrete Continuous Dyn. Syst. B* **25** 1141
- [49] Lutz E 2001 Fractional Langevin equation *Phys. Rev. E* **64** 051106
- [50] Jeon J-H, Leijne N, Oddershede L B and Metzler R 2013 Anomalous diffusion and power-law relaxation of the time averaged mean squared displacement in worm-like micellar solutions *New J. Phys.* **15** 045011
- [51] Tabei S M A, Burov S, Kim H Y, Kuznetsov A, Huynh T, Jureller J, Philipson L H, Dinner A R and Scherer N F 2013 Intracellular transport of insulin granules is a subordinated random walk *Proc. Natl Acad. Sci.* **110** 4911
- [52] Jeon J-H, Javanainen M, Martinez-Seara H, Metzler R and Vattulainen I 2016 Protein crowding in lipid bilayers gives rise to non-Gaussian anomalous lateral diffusion of phospholipids and proteins *Phys. Rev. X* **6** 021006
- [53] Lampo T J, Stylianidou S, Backlund M P, Wiggins P A and Spakowitz A J 2017 Cytoplasmic RNA-protein particles exhibit non-Gaussian subdiffusive behavior *Biophys. J.* **112** 532
- [54] Zan W, Xu Y, Kurths J, Chechkin A V and Metzler R 2020 Stochastic dynamics driven by combined Lévy–Gaussian noise: fractional Fokker–Planck–Kolmogorov equation and solution *J. Phys. A: Math. Theor.* **53** 385001
- [55] Ma J, Xu Y, Li Y, Tian R, Ma S and Kurths J 2021 Quantifying the parameter dependent basin of the unsafe regime of asymmetric Lévy-noise-induced critical transitions *Appl. Math. Mech. Engl. Ed.* **42** 65
- [56] Li Y, Xu Y and Kurths J 2017 Roughness-enhanced transport in a tilted ratchet driven by Lévy noise *Phys. Rev. E* **96** 052121
- [57] Li Y, Xu Y, Kurths J and Yue X 2016 Lévy-noise-induced transport in a rough triple-well potential *Phys. Rev. E* **94** 042222
- [58] Xu Y, Li Y, Zhang H, Li X and Kurths J 2016 The switch in a genetic toggle system with Lévy noise *Sci. Rep.* **6** 31505
- [59] Dubkov A A, Spagnolo B and Uchaikin V V 2008 Lévy flight superdiffusion: an introduction *Int. J. Bifurcation Chaos* **18** 2649
- [60] Dubkov A A and Spagnolo B 2008 Verhulst model with Lévy white noise excitation *Eur. Phys. J. B* **65** 361
- [61] Guarcello C, Valenti D, Carollo A and Spagnolo B 2016 Effects of Lévy noise on the dynamics of sine-Gordon solitons in long Josephson junctions *J. Stat. Mech.* **054012**
- [62] Wang B, Kuo J, Bae S C and Granick S 2012 When Brownian diffusion is not Gaussian *Nat. Mater.* **11** 481
- [63] Sokolov I M 2012 Models of anomalous diffusion in crowded environments *Soft Matter* **8** 9043
- [64] Beck C and Cohen E G D 2003 Superstatistics *Physica A* **322** 267
- [65] Beck C 2007 Statistics of three-dimensional Lagrangian turbulence *Phys. Rev. Lett.* **98** 064502
- [66] Massignan P, Manzo C, Torrena-Pina J A, García-Parajo M F, Lewenstein M and Lapeyre G J Jr 2014 Nonergodic subdiffusion from Brownian motion in an inhomogeneous medium *Phys. Rev. Lett.* **112** 150603
- [67] Luo L and Yi M 2019 Quenched trap model on the extreme landscape: the rise of subdiffusion and non-Gaussian diffusion *Phys. Rev. E* **100** 042136
- [68] Burov S and Barkai E 2020 Packets of spreading particles exhibit universal exponential tails *Phys. Rev. Lett.* **124** 060603
- [69] Lanoiselée Y, Moutal N and Grebenkov D 2018 Diffusion-limited reactions in dynamic heterogeneous media *Nat. Commun.* **9** 4398

- [70] Cherstvy A G and Metzler R 2016 Anomalous diffusion in time-fluctuating non-stationary diffusivity landscapes *Phys. Chem. Chem. Phys.* **18** 23840
- [71] Sposini V, Chechkin A V, Seno F, Pagnini G and Metzler R 2018 Random diffusivity from stochastic equations: comparison of two models for Brownian yet non-Gaussian diffusion *New J. Phys.* **20** 043044
- [72] Lanoiselée Y and Grebenkov D S 2018 A model of non-Gaussian diffusion in heterogeneous media *J. Phys. A: Math. Theor.* **51** 145602
- [73] Chubynsky M V and Slater G W 2014 Diffusing diffusivity: a model for anomalous and anomalous yet Brownian diffusion *Phys. Rev. Lett.* **113** 098302
- [74] Jain R and Sebastian K L 2016 Diffusion in a crowded, rearranging environment *J. Phys. Chem. B* **120** 3988
- [75] Tyagi N and Cherayil B J 2017 Non-Gaussian Brownian diffusion in dynamically disordered thermal environments *J. Phys. Chem. B* **121** 7204
- [76] Chechkin A V, Seno F, Metzler R and Sokolov I M 2017 Brownian yet non-Gaussian diffusion: from superstatistics to subordination of diffusing diffusivities *Phys. Rev. X* **7** 021002
- [77] Yamamoto E, Akimoto T, Mitsutake A and Metzler R 2021 Universal relation between instantaneous diffusivity and radius of gyration of proteins in aqueous solution *Phys. Rev. Lett.* **126** 128101
- [78] Hapca S, Crawford J W and Young I M 2009 Anomalous diffusion of heterogeneous populations characterized by normal diffusion at the individual level *J. R. Soc. Interface* **6** 111
- [79] Postnikov E B, Chechkin A and Sokolov I M 2020 Brownian yet non-Gaussian diffusion in heterogeneous media: from superstatistics to homogenization *New J. Phys.* **22** 063046
- [80] Ślęzak J, Burnecki K and Metzler R 2019 Random coefficient autoregressive processes describe Brownian yet non-Gaussian diffusion in heterogeneous systems *New J. Phys.* **21** 073056
- [81] Sabri A, Xu X, Krapf D and Weiss M 2020 Elucidating the origin of heterogeneous anomalous diffusion in the cytoplasm of mammalian cells *Phys. Rev. Lett.* **125** 058101
- [82] He W, Song H, Su Y, Geng L, Ackerson B J, Peng H B and Tong P 2016 Dynamic heterogeneity and non-Gaussian statistics for acetylcholine receptors on live cell membrane *Nat. Commun.* **7** 11701
- [83] Wang W, Seno F, Sokolov I M, Chechkin A V and Metzler R 2020 Unexpected crossovers in correlated random-diffusivity processes *New J. Phys.* **22** 083041
- [84] Wang W, Cherstvy A G, Chechkin A V, Thapa S, Seno F, Liu X and Metzler R 2020 Fractional Brownian motion with random diffusivity: emerging residual nonergodicity below the correlation time *J. Phys. A: Math. Theor.* **53** 474001
- [85] Ślęzak J, Metzler R and Magdziarz M 2019 Codifference can detect ergodicity breaking and non-Gaussianity *New J. Phys.* **21** 053008
- [86] Sposini V, Grebenkov D S, Metzler R, Oshanin G and Seno F 2020 Universal spectral features of different classes of random-diffusivity processes *New J. Phys.* **22** 063056
- [87] Grebenkov D S, Sposini V, Metzler R, Oshanin G and Seno F 2021 Exact distributions of the maximum and range of random diffusivity processes *New J. Phys.* **23** 023014
- [88] Cherstvy A G, Chechkin A V and Metzler R 2013 Anomalous diffusion and ergodicity breaking in heterogeneous diffusion processes *New J. Phys.* **15** 083039
- [89] Olivares-Rivas W, Colmenares P J and López F 2013 Direct evaluation of the position dependent diffusion coefficient and persistence time from the equilibrium density profile in anisotropic fluids *J. Chem. Phys.* **139** 074103
- [90] Hummer G 2005 Position-dependent diffusion coefficients and free energies from Bayesian analysis of equilibrium and replica molecular dynamics simulations *New J. Phys.* **7** 34
- [91] Li Y, Mei R, Xu Y, Kurths J, Duan J and Metzler R 2020 Particle dynamics and transport enhancement in a confined channel with position-dependent diffusivity *New J. Phys.* **22** 053016
- [92] Kühn T, Ihalainen T O, Hyväluoma J, Dross N, Willman S F, Langowski J, Vihinen-Ranta M and Timonen J 2011 Protein diffusion in mammalian cell cytoplasm *PLoS One* **6** e22962
- [93] English B P, Haurlyuk V, Sanamrad A, Tankov S, Dekker N H and Elf J 2011 *Proc. Natl Acad. Sci.* **108** E365
- [94] Cherstvy A G, Chechkin A V and Metzler R 2014 Particle invasion, survival, and non-ergodicity in 2D diffusion processes with space-dependent diffusivity *Soft Matter* **10** 1591
- [95] Cherstvy A G and Metzler R 2013 Population splitting, trapping, and non-ergodicity in heterogeneous diffusion processes *Phys. Chem. Chem. Phys.* **15** 20220

- [96] Leibovich N and Barkai E 2019 Infinite ergodic theory for heterogeneous diffusion processes *Phys. Rev. E* **99** 042138
- [97] Wang X, Deng W and Chen Y 2019 Ergodic properties of heterogeneous diffusion processes in a potential well *J. Chem. Phys.* **150** 164121
- [98] Burov S, Metzler R and Barkai E 2010 Aging and nonergodicity beyond the Khinchin theorem *Proc. Natl Acad. Sci.* **107** 13228
- [99] Wiesenfeld K, Pierson D, Pantazelou E, Dames C and Moss F 1994 Stochastic resonance on a circle *Phys. Rev. Lett.* **72** 2125
- [100] Nozaki D, Mar D J, Grigg P and Collins J J 1999 Effects of colored noise on stochastic resonance in sensory neurons *Phys. Rev. Lett.* **82** 2402
- [101] Mato G 1999 Stochastic resonance using noise generated by a neural network *Phys. Rev. E* **59** 3339
- [102] Frauenfelder H and Wolynes P 1985 Rate theories and puzzles of heme protein kinetics *Science* **229** 337
- [103] Stein D L 1985 A model of protein conformational substates *Proc. Natl Acad. Sci.* **82** 3670
- [104] Leibler S 1994 Moving forward noisily *Nature* **370** 412
- [105] Jung P and Hänggi P 1988 Bistability and colored noise in nonequilibrium systems: theory versus precise numerics *Phys. Rev. Lett.* **61** 11
- [106] Bray A J and McKane A J 1989 Instanton calculation of the escape rate for activation over a potential barrier driven by colored noise *Phys. Rev. Lett.* **62** 493
- [107] Leiber T, Marchesoni F and Risken H 1987 Colored noise and bistable Fokker–Planck equations *Phys. Rev. Lett.* **59** 1381
- [108] Dixit S N and Sahni P S 1983 Nonlinear stochastic processes driven by colored noise: application to dye-laser statistics *Phys. Rev. Lett.* **50** 1273
- [109] Lett P, Short R and Mandel L 1984 Photon statistics of a dye laser far below threshold *Phys. Rev. Lett.* **52** 341
- [110] Zhu S, Yu A W and Roy R 1986 Statistical fluctuations in laser transients *Phys. Rev. A* **34** 4333
- [111] Kubo R 1962 *Fluctuations, Relaxation and Resonance in Magnetic Systems* ed D ter Haar (Edinburgh: Edinburgh University Press)
- [112] Spanio T, Hidalgo J and Muñoz M A 2017 Impact of environmental colored noise in single-species population dynamics *Phys. Rev. E* **96** 042301
- [113] Müller-Hansen F, Droste F and Lindner B 2015 Statistics of a neuron model driven by asymmetric colored noise *Phys. Rev. E* **91** 022718
- [114] Xu Y, Liu X, Li Y and Metzler R 2020 Heterogeneous diffusion processes and non-ergodicity with Gaussian coloured noise in layered diffusivity landscapes *Phys. Rev. E* **102** 062106
- [115] Mei R, Xu Y, Li Y and Kurths J 2020 The steady current analysis in a periodic channel driven by correlated noises *Chaos Solitons Fractals* **135** 109766
- [116] Zhang X, Xu Y, Liu Q and Kurths J 2020 Rate-dependent tipping-delay phenomenon in a thermoacoustic system with colored noise *Sci. China Tech. Sci.* **63** 2316
- [117] Yue X, Wang Y, Han Q, Xu Y and Xu W 2019 Transient responses of nonlinear dynamical systems under colored noise *Europhys. Lett.* **127** 24004
- [118] Mantegna R N and Spagnolo B 1995 Stochastic resonance in a tunnel diode in the presence of white or coloured noise *Il Nuovo Cimento D* **17** 873
- [119] Valenti D, Augello G and Spagnolo B 2008 Dynamics of a FitzHugh–Nagumo system subjected to autocorrelated noise *Eur. Phys. J. B* **65** 443
- [120] Liu D, Xu Y and Li J 2017 Probabilistic response analysis of nonlinear vibration energy harvesting system driven by Gaussian colored noise *Chaos Solitons Fractals* **104** 806
- [121] Zhang H, Xu Y and Xu W 2009 Approximate stationary solution and stochastic stability for a class of differential equations with parametric colored noise *Nonlinear Dyn.* **56** 213
- [122] Xu Y, Zhang H and Xu W 2007 On stochastic complex beam–beam interaction models with Gaussian colored noise *Physica A* **384** 259
- [123] Lehle B and Peinke J 2018 Analyzing a stochastic process driven by Ornstein–Uhlenbeck noise *Phys. Rev. E* **97** 012113
- [124] Picolo S, Mendes R S, Malacarne L C and Santos R P B 2009 q -distributions in complex systems: a brief review *Braz. J. Phys.* **39** 468
- [125] Budini A 2015 Extended q -Gaussian and q -exponential distributions from gamma random variables *Phys. Rev. E* **91** 052113
- [126] Tsallis C 1988 Possible generalization of Boltzmann–Gibbs statistics *J. Stat. Phys.* **52** 479
- [127] Tsallis C 2009 *Introduction to Nonextensive Statistical Mechanics* (New York: Springer)

- [128] Tsallis C and Bukman D J 1996 Anomalous diffusion in the presence of external forces: exact time-dependent solutions and their thermostistical basis *Phys. Rev. E* **54** R2197
- [129] Tsallis C, Anteneodo C, Borland L and Osorio R 2003 Nonextensive statistical mechanics and economics *Physica A* **324** 89
- [130] Borland L and Bouchaud J-P 2004 A non-Gaussian option pricing model with skew *Quant. Finance* **4** 499
- [131] Marini U, Marconi B and Puglisi A 2002 Mean-field model of free-cooling inelastic mixtures *Phys. Rev. E* **65** 051305
- [132] Caruso F, Pluchino A, Latora V, Vinciguerra S and Rapisarda A 2007 Analysis of self-organized criticality in the Olami–Feder–Christensen model and in real earthquakes *Phys. Rev. E* **75** 055101(R)
- [133] Rodríguez A, Schwämmle V and Tsallis C 2008 Strictly and asymptotically scale invariant probabilistic models of N correlated binary random variables having q -Gaussians as $N \rightarrow \infty$ limiting distributions *J. Stat. Mech.* P09006
- [134] Castro F J, Kuperman N M, Fuentes M and Wio H S 2001 Experimental evidence of stochastic resonance without tuning due to non Gaussian noises *Phys. Rev. E* **64** 051105
- [135] Fuentes M A, Wio H S and Toral R 2002 Effective Markovian approximation for non-Gaussian noises: a path integral approach *Physica A* **303** 91
- [136] Wio H S 2005 Noise induced phenomena and nonextensivity *Europhys. News* **36** 197
- [137] Hänggi P and Jung P 1995 Colored noise in dynamical systems *Adv. Chem. Phys.* **89** 239
- [138] Xu Y, Zan W, Jia W and Kurths J 2019 Path integral solutions of the governing equation of SDEs excited by Lévy white noise *J. Comput. Phys.* **394** 41
- [139] Jung P and Hänggi P 1987 Dynamical systems: a unified colored-noise approximation *Phys. Rev. A* **35** 4464
- [140] Hasegawa H 2007 A moment approach to non-Gaussian colored noise *Physica A* **384** 241
- [141] Deza J I and Deza R R 2018 q noise: a generator of non-Gaussian colored noise (arXiv:1812.07451)
- [142] Wio H S 2004 On the role of non-Gaussian noises on noise-induced Phenomena *Nonextensive Entropy: Interdisciplinary Applications* ed M Gell-Mann and C Tsallis (Oxford: Oxford University Press)
- [143] Lau A W C and Lubensky T C 2007 State-dependent diffusion: thermodynamics consistency and its path integral formulation *Phys. Rev. E* **76** 011123
- [144] Volpe G and Wehr J 2016 Effective drifts in dynamical systems with multiplicative noise: a review of recent progress *Rep. Prog. Phys.* **79** 053901
- [145] He Y, Burov S, Metzler R and Barkai E 2008 Random time-scale invariant diffusion and transport coefficients *Phys. Rev. Lett.* **101** 058101
- [146] Lebowitz J L and Penrose O 1973 Modern ergodic theory *Phys. Today* **26** 23
- [147] Burov S, Jeon J-H, Metzler R and Barkai E 2011 Single particle tracking in systems showing anomalous diffusion: the role of weak ergodicity breaking *Phys. Chem. Chem. Phys.* **13** 1800
- [148] Schulz J H P, Barkai E and Metzler R 2014 Aging renewal theory and application to random walks *Phys. Rev. X* **4** 011028
- [149] Deng W and Barkai E 2009 Ergodic properties of fractional Brownian–Langevin motion *Phys. Rev. E* **79** 011112
- [150] Rytov S M, Kravtsov Y A and Tatarskii V I 1987 *Principles of Statistical Radiophysics 1: Elements of Random Process Theory* (Heidelberg: Springer)
- [151] Godec A and Metzler R 2013 Finite-time effects and ultraweak ergodicity breaking in superdiffusive dynamics *Phys. Rev. Lett.* **110** 020603
- [152] Li S and Huang J 2020 Non-Gaussian noise induced stochastic resonance in FitzHugh–Nagumo neural system with time delay *AIP Adv.* **10** 025310
- [153] Zhang H, Xu W and Xu Y 2009 The study on a stochastic system with non-Gaussian noise and Gaussian colored noise *Physica A* **388** 781
- [154] Spiechowicz J, Hänggi P and Luczka J 2009 Coexistence of absolute negative mobility and anomalous diffusion *New J. Phys.* **21** 083029